An ecosystem model of the global ocean including Fe, Si, P colimitations

Olivier Aumont,[1] Ernst Maier-Reimer,[2] Stéphane Blain,[3] and P. Monfray[4]

[1]   Observations have shown that large areas of the world ocean are characterized by lower than expected chlorophyll concentrations given the ambient phosphate and nitrate levels. In these High Nutrient-Low Chlorophyll regions, limitations of phytoplankton growth by other nutrients like silicate or iron have been hypothesized and further evidenced by in situ experiments. To explore these limitations, a nine-component ecosystem model has been embedded in the Hamburg model of the oceanic carbon cycle (HAMOCC5). This model includes phosphate, silicate, dissolved iron, two phytoplankton size fractions (nanophytoplankton and diatoms), two zooplankton size fractions (microzooplankton and mesozooplankton), one detritus and semilabile dissolved organic matter. The model is able to reproduce the main characteristics of two of the three main HNLC areas, i.e., the Southern Ocean and the equatorial Pacific. In the subarctic Pacific, silicate and phosphate surface concentrations are largely underestimated because of deficiencies in ocean dynamics. The low chlorophyll concentrations in HNLC areas are explained by the traditional hypothesis of a simultaneous iron-grazing limitation: Diatoms are limited by iron whereas nanophytoplankton is controlled by very efficient grazing by microzooplankton. Phytoplankton assimilates 18×10^9 mol Fe yr^{-1} of which 73% is supplied by regeneration within the euphotic zone. The model predicts that the ocean carries with it about 75% of the phytoplankton demand for new iron, assuming a 1% solubility for atmospheric iron. Finally, it is shown that a higher supply of iron to surface water leads to a higher export production but paradoxically to a lower primary productivity.   *INDEX TERMS:* 1050 Geochemistry: Marine geochemistry (4835, 4850); 4815 Oceanography: Biological and Chemical: Ecosystems, structure and dynamics; 4842 Oceanography: Biological and Chemical: Modeling; 4845 Oceanography: Biological and Chemical: Nutrients and nutrient cycling; *KEYWORDS:* ocean, ecosystem, models, colimitations, global scale

1.   Introduction

[2]   Until recently, the magnitude of the biological pump was thought to be predominantly controlled by the availability of macronutrients nitrate and phosphate and by sunlight levels. In particular, when sunlight is sufficient, there is generally a positive correlation between macronutrients concentrations and phytoplankton biomass, at least in open ocean ecosystems. However, in three major areas of the world ocean, that is the subarctic Pacific, the eastern and central equatorial Pacific, and the Southern Ocean, this common view does not seem to hold. Elevated nitrate and phosphate concentrations persist throughout the year in surface waters with relatively modest phytoplankton levels. These regions of "lower than expected" chlorophyll have been termed high nutrient-low chlorophyll (HNLC) [e.g., *Martin and Fitzwater*, 1988; *de Baar et al.*, 1990].

[3]   Three main hypothesis have been proposed to explain the paradox of these areas. First, phytoplankton growth may be limited by other nutrients than phosphate or nitrate, in particular by the micronutrient iron [*Martin and Fitzwater*, 1988]. This iron limitation hypothesis has been then supported by local iron enrichment experiments in the equatorial Pacific (IRONEX II [*Coale et al.*, 1996]) and in the Southern Ocean (SOIREE [*Boyd et al.*, 2000]). Because of the requirement diatoms have for silicon, silicate may also play a key role, either in the equatorial Pacific ocean [*Dugdale and Wilkerson*, 1998] or in the Antarctic Circumpolar Current [*Jacques*, 1983; *Sommer*, 1986]. Second, a high grazing pressure may remove a substantial part of the phytoplankton biomass [*Frost*,

---

[1]Laboratoire d'Océanographie Dynamique et de Climatologie, Paris, France.
[2]Max-Planck Institut fuer Meteorologie, Hamburg, Germany.
[3]Institut Universitaire Européen de la Mer, Plouzané France.
[4]Laboratoire des Sciences du Climat et de l'Environnement, Gif-sur-Yvette, France.

1991]. Finally, unfavorable light-mixing regime may prevent phytoplankton from blooming, especially in the Southern Ocean where the summer mixed layer depth is about 60–120 m [*Nelson and Smith*, 1991]. In fact, the consensus is now that iron or silicate is limiting the growth of large cells, mainly diatoms [*Chavez et al.*, 1991; *Fitzwater et al.*, 1996]. The predominant small-sized phytoplankton which has low iron requirement is maintained at modest levels by efficient grazing by microzooplankton [*Landry et al.*, 1995; *Verity et al.*, 1996].

[4] Because of the potential crucial role iron has in the ocean biological pump, there has been in the recent years an increasing interest in the biogeochemical cycling of iron [e.g., *Johnson et al.*, 1997; *Gerringa et al.*, 2000]. Thanks to the increasing amount of iron data [e.g., *Martin et al.*, 1993; *de Baar et al.*, 1999; *Sohrin et al.*, 2000], the iron distribution has been shown to exhibit a nutrient-like vertical distribution with very low concentrations in the euphotic zone and much higher levels in the subsurface and deep ocean [*Johnson et al.*, 1997]. However, iron shows remarkable features as emphasized by *Johnson et al.* [1997]. First, iron differs from other nutrients like nitrate or phosphate in the sense that its concentrations does not increase from the North Atlantic deep waters to the North Pacific deep waters. Second, unlike rapidly scavenged elements like aluminum or manganese, iron distribution does not exhibit decreasing concentrations with depth and as the age of water masses increases from the North Atlantic to the North Pacific.

[5] These remarkable patterns have lead *Johnson et al.* [1997] to hypothesize that iron scavenging is strongly reduced below 0.6 nM, which seems to be approximately an upper limit for iron concentrations in the deep open ocean. This reduction may be due to complexation of dissolved iron by strong organic ligands with this capacity of about 0.6 nM. In fact, observations have found such a strong class of chelators both in the Atlantic and in the Pacific ocean [*Wu and Luther*, 1995; *Rue and Bruland*, 1995]. Furthermore, recent studies have also shown that most of the dissolved iron in open ocean waters is bound to strong organic ligands [*van den Berg et al.*, 1995; *Nolting et al.*, 1998]. *Johnson et al.* [1997] suggested an alternative mechanism to explain these relatively constant iron concentrations in the deep ocean: a chemical equilibrium between the dissolved and particulate phases of iron. However, none of these mechanisms is yet certain.

[6] New iron is supplied to surface waters by three different sources. By new iron, we mean iron that is not regenerated within the euphotic zone (similar to the concept of new production as defined by *Eppley and Peterson* [1979]). The first source is atmospheric deposition from mineral dusts. This supply is hypothesized to be dominant for the open ocean, especially because HNLC regions are generally remote areas with very low dust deposition [*Duce and Tindale*, 1991]. The second source is the vertical supply of iron from below the euphotic zone by advection or vertical mixing, that may dominate in areas of deep convection, like the Southern Ocean and the North Atlantic, and in regions of strong upwelling, for instance the equatorial Pacific. Finally, iron is supplied to the ocean from

rivers and continental-shelf sediments. Because of the relatively short lifetime of iron in surface waters, this source is thought to be relatively minor for the open ocean (but not for coastal zones). However, satellite data have shown large chlorophyll concentrations near the Kerguelen Island in the Southern Ocean which suggest that this natural iron enrichment by land may be important even in open ocean [*Blain et al.*, 2001]. On global scale, the relative importance of those different sources of iron for the biological pump is not known and under debate. Based on models, *Archer and Johnson* [2000] and *Moore et al.* [2002a] have estimated that about 70–80% of the new iron is originating from the subsurface. On the other hand, from observation and model results, *Fung et al.* [2000] found that atmospheric deposition is dominant, representing up to 93% of the total supply of new iron. All these studies ignored the coastal supply of iron.

[7] Models represent a powerful tool to understand the ocean carbon-cycle and the role of the biological pump of CO_2. In the global ocean carbon-cycle model class, only one limiting nutrient and one generic phytoplankton compartment are generally modeled. Thus, these models are not suitable for HNLC areas, where they simulate much too high phytoplankton biomasses [*Six and Maier-Reimer*, 1996; *Aumont et al.*, 2002; *Palmer and Totterdell*, 2001]. Models with multiple limiting nutrients (generally iron/nitrogen or iron/nitrogen/silicon) have been used in 1-D configurations [*Pondaven et al.*, 1998; *Leonard et al.*, 1999; *Lancelot et al.*, 2000] and in a 3-D regional model of the equatorial Pacific ocean [*Christian et al.*, 2002]. Very recently, a model with four limiting nutrients (nitrogen/phosphorus/iron/silicon) has been developed in a 1-D configuration [*Moore et al.*, 2002b] and then applied to the global scale [*Moore et al.*, 2002a]. To our knowledge, this study is the first attempt to model multiple colimitations on the global scale with such a detailed model. However, this work is not based on a true 3-D coupled biogeochemical/dynamical model of the global ocean as the ecosystem model is embedded in a physical mixed-layer grid. Thus no horizontal transport is considered and a simplified treatment of vertical transport is applied. In this paper, we discuss the results of a global 3-D ocean-carbon cycle model which includes colimitation by phosphate, iron and silicate. The ecosystem model is based on two phytoplankton size-classes (pico-/nanophytoplankton and diatoms) and two zooplankton size-classes (microzooplankton and mesozooplankton). In a first step, the behavior of the model is evaluated with available observations. Then, the role of the different limiting nutrients and phytoplankton classes are analyzed. Finally, the budget of iron in the photic zone is more extensively examined.

2. Model Description

[8] The HAMOCC5 model is based on an off-line version of the Hamburg Large Scale Geostrophic model (LSG) of the global ocean with realistic topography [*Maier-Reimer et al.*, 1993]. The horizontal resolution is uniformly 3.5 by 3.5 degrees. The model has 22 vertical layers, whose thickness
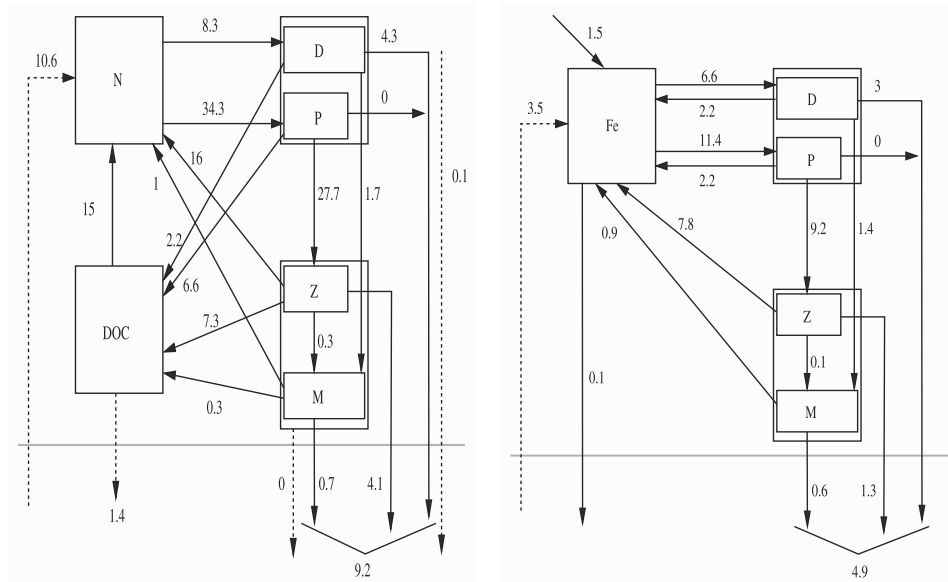
Figure 1.   Annual mean nutrients fluxes between the modeled compartments of HAMOCC5. Left panel corresponds to carbon fluxes (in Gt C yr^{-1}). Right panel shows the iron fluxes (in 10^9 mol Fe yr^{-1}). The bottom limit of the productive zone is set to 100 m in the model.

varies from 50 m at the surface to 800 m at the bottom of the ocean (set to 6000 m). The LSG model provides monthly mean fields of advection, convective events, temperature and salinity, which are used to simulate the spatial and temporal distribution of the tracers. These fields, except for convective events, are linearly interpolated onto the temporal resolution of the biological model, which is set to 3 days. Convection is applied once a month with special treatment of phytoplankton growth (see below) to avoid numerical instabilities. Advective transport of tracers is computed using an upstream scheme.

[9] The HAMOCC5 model is derived from the HAMOCC3.1 model described by *Six and Maier-Reimer* [1996]. The main difference is the limitation of the autotrophic activity not only by phosphate but also by iron and silicate. These additional limitations have required to split the original generic phytoplankton reservoir into two distinct compartments corresponding to pico-/nanophytoplankton and diatoms, the latter requiring silicate and high level of iron for growth. Accordingly, two size-classes of zooplankton have been distinguished, the microzooplankton and the mesozooplankton. Thus the ecosystem model now includes eleven compartments (see Figure 1): phosphate (N), silicic acid (Si), and iron (Fe) as colimiting nutrients, nanophytoplankton (P), diatoms (D) and silicon content of diatoms (D*), microzooplankton (Z) and mesozooplankton (M), dissolved organic carbon (DOC), particulate organic carbon (POC) and iron content of POC (PFe).The governing equations are given in Table 1. POC and PFe are considered to be only nonliving particles. Particles produced in the euphotic zone are instantaneously exported into the intermediate and deep ocean with a prescribed power-law profile [*Suess*, 1980]. DOC in the model is supposed to represent the semilabile component of the dissolved organic carbon pool. This compound has been shown to be potentially important for horizontal and vertical export of nutrients and carbon [*Carlson et al.*, 1994] as well as for seasonal storage of nutrients [*Bodungen and Kahler*, 1994]. In addition to the ecosystem model, HAMOCC5 also simulates dissolved inorganic carbon (DIC), total alkalinity (TALK) and oxygen (O2).

2.1.   Biogeochemical Model

[10] In this section, we only describe the new parameterizations adopted to model the iron and silicon cycles and the modifications that were necessary to incorporate their effects on marine productivity. Since most of the other parameterizations used in HAMOCC5 are common to other models, they are simply listed in Table 2 with the appropriate references the reader could refer to for further information.

[11] The temporal and spatial distribution of the incoming light I_0 is prescribed from monthly climatological fields constructed from 8 years of 12-hour weather analyses from the European Centre for Medium-Range Weather Forecasts (ECMWF). No light penetration is assumed through the sea-ice cover predicted by the LSG model. In addition to light limitation, a parameterization of Lagrangian production inhibition in case of deep mixing proposed by *André* [1990] has been included. As shown by *Lévy et al.* [1998], such parameterization improves model prediction. Here, only two cases are considered: When the mixed layer depth, the vertical extent of the convective mixing in the LSG model, is shallower than the euphotic zone, phytoplankton growth rate is not reduced (L_m = 1); in the opposite case, phytoplankton growth is reduced by 90% (L_m = 0.1). In work by *André* [1990], a transitory case is considered when the mixed layer depth is comprised between the euphotic depth and twice the depth

Table 1. Source/Sink Budget Due to Biogeochemical Processes in the Top 100 m of the Ocean Model

Sources/Sinks	
$S(P)$	$\mu^P L_m L_P P - m_P \frac{(P-P_{min})}{K_P+P} P - g_Z(P)Z - \gamma_P(P - P_{min})$
$S(D)$	$\mu^D L_m L_D D - m_D \frac{(D-D_{min})}{K_D+D} D - g_M(D)M - \gamma_D(D - D_{min})$
$S(D^\star)$	$\left(\frac{Si}{C}\right)\mu^D L_m L_D D^\star - m_D \frac{D}{K_D+D} D^\star - g_M(D)\frac{D^\star}{D} M - \gamma_D \frac{D^\star}{D}(D - D_{min})$
$S(Z)$	$\epsilon_Z \sigma_Z g_Z(P)Z - m_Z(Z - Z_{min}) - \gamma_Z(Z - Z_{min}) - g_M(Z)M$
$S(M)$	$\epsilon_M \sigma_M(g_M(D) + g_M(Z))M - m_M(M - M_{min}) - \gamma_M(M - M_{min})$
$S(DOC)$	$\gamma_P(P - P_{min})P + \gamma_D(D - D_{min})D + \gamma_Z(Z - Z_{min}) + \gamma_M(M - M_{min}) - r_{doc}(N)\,DOC$
$S(POC)$	$F_1 - r_{poc}POC$
$R_{C:P}S(N)$	$-\mu^P L_m L_P P - \mu^D L_m L_D D + \sigma_Z(1 - \epsilon_Z)g_Z(P)Z + m_Z(Z - Z_{min}) + \sigma_M(1 - \epsilon_M)(g_M(D) + g_Z(Z))M + m_M \epsilon_{can}(M - M_{min}) + r_{doc}(N)DOC$
	$+ r_{poc}POC$
$S(Si)$	$-\left(\frac{Si}{C}\right)\mu^D L_m L_D D^\star + r(Si)$
$S(Fe)$	$\left(\frac{Fe}{C}\right)^P(-\mu^P L_m L_P P + \gamma_P(P - P_{min}) + \gamma_Z(Z - Z_{min}) + \gamma_M(M - M_{min}) + m_M(1 - \epsilon_{can})(M - M_{min}) + \sigma_Z(1 - \epsilon_Z)g_Z(P)Z$
	$+ \sigma_M(1 - \epsilon_M)g_M(Z)M + \left(\frac{Fe}{C}\right)^D(-\mu^D L_m L_D D + \sigma_M(1 - \epsilon_M)g_M(D)M + \gamma_D(D - D_{min})D) + \left(\frac{Fe}{C}\right)^P - \left(\frac{Fe}{C}\right)^D \epsilon_M \sigma_M g_M(D)M$
	$+ r_{poc}PFe - \lambda_{scav}\max(0, (Fe - 0.6\,nM))$
$S(PFe)$	$G(P, D, Z, M, z) - r_{poc}PFe$

of the euphotic zone. Furthermore, because of the crude vertical resolution of the LSG model, the euphotic depth is set uniformly to 100 m over the global ocean, that is the depth of the productive zone.

[12] It has been suggested that sinking of diatoms may be favored by silicate or iron starvation [*Muggli et al.*, 1996]. Since in our model, no sinking is considered for phytoplanktonic cells, we mimic this net loss by increasing

Table 2. Source/Sink Terms for Phytoplankton and Zooplankton

Process	Equation	Reference
	Phytoplankton	
Growth rate	$\mu = \frac{f(T)f(L)}{\sqrt{f(T)^2+f(L)^2}}$	*Jassby and Platt* [1976]
Light limitation	$f(L) = I_0 \alpha PAR \frac{1}{z}\int_z e^{-kz}dz$	
Temperature dependence	$f(T) = ab^{cT}$	*Eppley* [1972]
Nutrient limitation for P	$L_P = \min\left(\frac{N}{K_N^P+N}, \frac{Fe}{K_{Fe}^P+Fe}\right)$	
Nutrient limitation for D	$L_D = \min\left(\frac{N}{K_N^D+N}, \frac{Fe}{K_{Fe}^D+Fe}, \frac{Si}{K_{Si}^D+Si}\right)$	
Chl/C in phytoplankton	$\frac{Chl^\star}{C} = \left(\frac{Chl}{C^M} - \left(\frac{Chl^M}{C} - \frac{Chl^m}{C}\right)\min\left(\frac{L}{I_{par}^{max}}, 1\right)\right)L_{P,D}$	*Doney et al.* [1996]
	Microzooplankton	
Grazed nanophytoplankton	$g_Z(P) = g_Z \frac{P}{K_Z+P}$	*Fasham et al.* [1990]
	Mesozooplankton	
Grazed diatoms	$g_M(D) = g_M \frac{p_D D}{K_M+p_D D+p_Z Z}$	*Fasham et al.* [1990]
Grazed microzooplankton	$g_M(Z) = g_M \frac{p_Z Z}{K_M+p_D D+p_Z Z}$	*Fasham et al.* [1990]
Preference for diatoms	$p_D = \frac{\pi_D D}{\pi_D D+\pi_Z Z}$	*Fasham et al.* [1990]
Preference for Z	$p_Z = \frac{\pi_Z Z}{\pi_D D+\pi_Z Z}$	*Fasham et al.* [1990]
	DOC	
Remineralization rate	$r_{doc}(N) = d_0 \frac{N}{N+k_d}$	*Six and Maier-Reimer* [1996]
	POC	
Export	$F_1 = (TPP_1 + TPP_2)\frac{\partial}{\partial z}\left(\frac{z}{100}\right)^{-0.8}$	*Suess* [1980]
Phytoplankton POC	$TPP_1 = \int_0^{100m}\left(m_P \frac{(P-P_{min})}{K_P+P}P + m_D \frac{(D-D_{min})}{K_D+D}D\right)dz$	
Zooplankton POC	$TPP_2 = \int_0^{100m}((1 - \sigma_Z)g_Z(P)Z + (1 - \sigma_M)(g_M(D) + g_Z(Z))M + m_M(1 - \varepsilon_{can})(M - M_{min}))dz$	
	Silicate	
Export	$r(Si) = TSI \frac{\partial}{\partial z}\left(e^{-\frac{z}{6km}}\right)$	*Maier-Reimer* [1993]
Biogenic Si Production	$TSI = \int_0^{100m}\left(m_D \frac{D}{K_D+D}D^\star + g_M(D)\frac{D^\star}{D}M + \gamma_D \frac{D^\star}{D}(D - D_{min})\right)dz$	

mortality to a threshold value when iron or silicate concentrations tend to zero:

$$m_D = m_{min} \quad \text{if } Si > K_{Si}^D \text{ and } Fe > K_{Fe}^D$$

$$m_D = m_{max} + (m_{min} - m_{max})\max\left(\frac{\frac{Si}{K_{Si}^D}}{,}\frac{\frac{Fe}{K_{Fe}^D}}{}\right)$$

$$\text{if } Si \leq K_{Si}^D \text{ and } Fe \leq K_{Fe}^D \quad (1)$$

where m_{min} and m_{max} are respectively the minimum and maximum diatoms specific mortality rates. The maximum sinking speed of nutrient-starved diatoms can reach 10 m d^{-1} [*Smetacek*, 1985]. Related to the thickness of the upper layers of the LSG model (50 m), this speed leads to a maximum loss rate of 0.2 d^{-1}.

[13] Observations have shown that the $\frac{Si}{C}$ ratio is not constant over the ocean. In particular, diatoms in subtropical and tropical areas, where ambient silicic acid concentrations are often below 1 µmol L^{-1}, may have $\frac{Si}{C}$ ratio five times as low as in Si-replete areas [e.g., *Brzezinski*, 1992]. Furthermore, this ratio seems to increase in iron-limited regions by up to three or four times [e.g., *Franck et al.*, 2000]. Thus, we have adopted the following very simple formulation to describe the $\frac{Si}{C}$ ratio for silicon uptake rate:

$$\left(\frac{Si}{C}\right) = \left(\frac{Si}{C}\right)^{av} \min\left(1., \frac{Si}{K_{si}}\right)\left(4. - 3 \times \min\left(1., \frac{Fe}{K_{Fe}^D}\right)\right) \quad (2)$$

where $\left(\frac{Si}{C}\right)^{av}$ is the mean value of this ratio as proposed by *Nelson et al.* [1995] for the global ocean.

[14] Experimental data have shown that the half-saturation constant for diatom growth varies greatly over the ocean [e.g., *Nelson and Treguer*, 1992]. Putting these data together, *Pondaven et al.* [1999] have found a significant linear relationship between the value of K_{si}^D and the ambient silicic acid concentration. For instance, in the North Atlantic ocean, this constant is around 1 µmol Si L^{-1} whereas in the silicate-rich Southern Ocean, values are much higher ranging between 4 and almost 90 µmol Si L^{-1}. However, in the latter region, observations may be biased to high values because of a possible iron limitation. In vivo experiments generally show values between 1 and 8 µmol Si L^{-1}, varying with the ambient silicic acid concentration (A. Laynaert, personal communication, 2001). Thus, in HAMOCC5, we have adopted an alternative parameterization to that proposed by *Pondaven et al.* [1999] to account for an upper bound of 8 µmol Si L^{-1}:

$$K_{Si}^D = 0.8 + 7.2 \frac{Si}{K_{Si}^{\star} + Si} \quad (3)$$

where $K_{Si}^{\star}$ is set to 30 µmol Si L^{-1}, a high value which ensures an almost linear behavior for small Si concentrations as given by *Pondaven et al.* [1999].

[15] The equation for iron changes is given in Table 1 (S(Fe)). This rather long equation is based on two assumptions. First, all the dissolved iron in seawater is supposed to be bioavailable for phytoplankton uptake. Thus, no distinction is made between the different forms of dissolved iron (for instance, between free, complexed and colloidal iron). Second, particulate organic iron (PFE) is assumed to be remineralized at the same rate as POC, as suggested by comparison between iron, nitrate and phosphate profiles [*Johnson et al.*, 1997]. Finally, because mesozooplankton and diatoms do not have the same $\frac{Fe}{C}$, iron conservation required a special treatment for grazing. The excess iron taken up by mesozooplankton on diatoms is released to the dissolved iron pool in surface waters. Indeed mesozooplankton can adjust their iron content by directly excreting excess iron. Dissolved iron in the water is not allowed to fall below 0.02 nM which is the minimum detection limit for dissolved iron.

[16] The $\frac{Fe}{C}$ ratio is quite difficult to evaluate and shows high variability over the ocean. The iron requirement for photosynthesis varies with species, iron availability, and light levels [*Sunda and Huntsman*, 1997]. Generally, nanophytoplankton has a lower requirement for dissolved iron than diatoms. Furthermore, diatoms seem to be able to adapt their iron need to the local availability in iron. Finally, iron uptake rates do not seem to be sensitive to light levels [*Sunda and Huntsman*, 1997]. In other words, at the bottom of the euphotic zone, phytoplanktonic cells increase their $\frac{Fe}{C}$ to maintain their maximum possible iron uptake rate. This increase induces higher removal rates of iron relative to other nutrients leading to higher Fe limitation, especially in surface waters.

[17] For all species except for diatoms, we have adopted a constant $\left(\frac{Fe}{C}\right)^P$ ratio set to a slightly higher value (4×10^{-6} µmol Fe mol C) than the minimum ratio needed for cell maintenance (3×10^{-6} µmol Fe mol C) inferred by *Sunda and Huntsman* [1997]. For diatoms, we assumed the following empirical relationship based on the previous considerations:

$$\left(\frac{Fe}{C}\right)^D = \left(\frac{Fe}{C}\right)^{min} + \frac{\left(\frac{Fe}{C}\right)^{\star}\frac{Fe}{K_{Fe}^{D+Fe}}}{\frac{f(L)}{\sqrt{f(L)^2 + f(T)^2}}} \quad (4)$$

where the denominator on the right hand side of this equation denotes the light effect, the numerator represents the effect of the availability in iron on the $\frac{Fe}{C}$ ratio. The expression for the light effect has been chosen to remove the light impact on the iron uptake rate by diatoms without changing the minimum requirement for cell maintenance. To avoid infinite values in case of no light (f(L) = 0), we set an upper bound of 1/30000 to this ratio.

[18] Iron, like other seawater metals (i.e., aluminium), is subject to scavenging by adsorption onto particles or precipitation. However, unlike these metals, observations suggest that the scavenging rates of iron should strongly decrease for concentrations below that 0.6 nM limit as iron concentrations rarely exceed that value in the open ocean [*Johnson et al.*, 1997]. To account for Fe scavenging, we have adopted the simple numerical model proposed by *Johnson et al.* [1997]:

$$S_{Fe} = \lambda_{scav} \max(0, (Fe - 0.6nM)) \quad (5)$$

[19] Based on numerical experiments using this parameterization, *Johnson et al.* [1997] has estimated λ_{scav} to $\frac{1}{200yr}$,
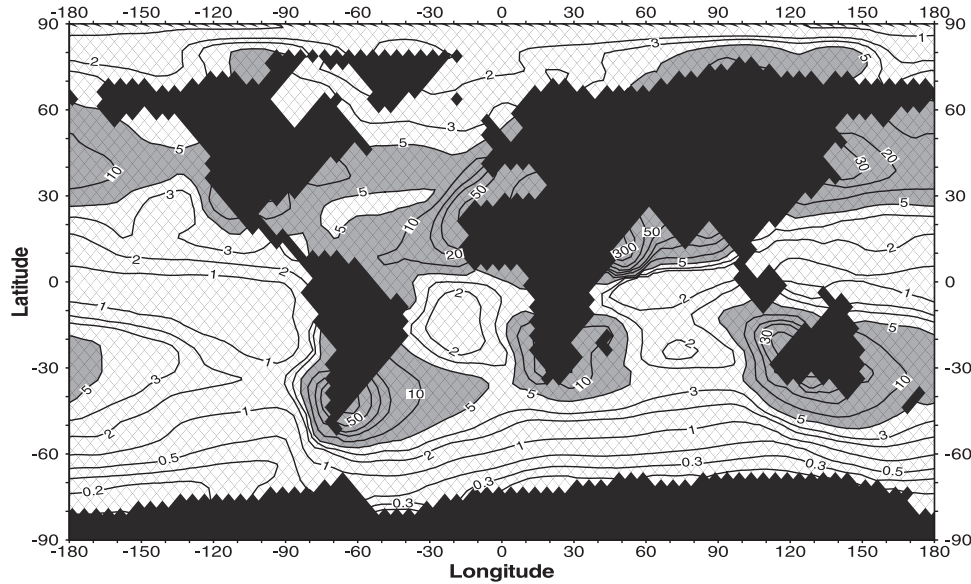
Figure 2. Annual mean atmospheric deposition of iron to surface waters from *Tegen and Fung* [1995]. Units are μmol Fe m^{-2} yr^{-1}. Shaded areas are for values above 5 μmol Fe m^{-2} yr^{-1}.

which is of the order of the estimated lifetime of iron in the ocean [*Bruland et al.*, 1994]. However, since a major process for iron scavenging is adsorption onto particles [*Archer and Johnson*, 2000], scavenging rates are likely to be related to the particle load of seawater. Thus we suggest the following parameterization for λ_{scav}:

$$\lambda_{scav} = \lambda_{scav}^0 + \lambda_{scav}^\star (P + D + Z + M + POC) \qquad (6)$$

where λ_{scav}^0 is the minimum scavenging rate set in HAMOCC5 to the value proposed by *Johnson et al.* [1997] for deep ocean scavenging rates, where the particle load is the lowest. $\lambda_{scav}^\star$ has been determined by a set of sensitivity experiments to avoid very high accumulation in the subsurface equatorial Pacific ocean (see for instance *Archer and Johnson* [2000, Figure 4]) and in areas of high particle deposition from the atmosphere. We are aware that this parameterization is very simplistic, partly because it does not account for crustal particles that may also enhance removal rates of iron from surface waters, especially in areas of intense aeolian input.

[20] In our standard simulation, we considered only atmospheric deposition of iron. We used the global monthly deposition maps from the *Tegen and Fung* [1995] dust model (Figure 2). Following *Fung et al.* [2000], we have assumed a relative iron content of 5% in silt particles and 1.2% in clay particles. However, all the iron deposited to the ocean is not readily available for biology. Based on a compilation of observations and on model budgets, *Jickells and Spokes* [2001] have estimated that between 0.8% and 2.1% of the deposited iron is rapidly soluble in seawater and thus, may be bioavailable. This range is significantly lower than the 10% bioavailability used by *Duce and Tindale* [1991]. Here we have used a 1% solubility for deposited iron, an intermediate value inside the range given by *Jickells and Spokes*

[2001]. Using these numbers for solubility and iron abundance in mineral aerosols, the total Fe deposition rates to the ocean surface were 149.7×10^9 mol yr^{-1}, of which about 1.5×10^9 mol yr^{-1} are available for phytoplankton uptake.

2.2. Initial Conditions and Model Integration

[21] Biological parameters and their values are listed in Table 3. The model uses only one set of parameter values for the global ocean. When available, these values have been taken from the literature. However, some not very well constrained (or even unknown) parameters have been adjusted within a "reasonable" range of values to achieve consistency with observations (for instance, the zooplankton mortality rates). This adjustment has been performed by successive model runs.

[22] We started the biological run from fields of HAMOCC3.1 [*Six and Maier-Reimer*, 1996]. Both phytoplankton size-classes and zooplankton size-classes have been initialized with values from generic phytoplankton and zooplankton distributions simulated by HAMOCC3.1. Fe has been set to the observed mean deep ocean value (0.6 nM) everywhere. PFe has been inferred from POC distribution using a constant conversion ratio of 5 μmol Fe (mol C)$^{-1}$. The model has been integrated for 4000 years. At this state, it is close to equilibrium with global primary production drifting by less than 0.001 GtC yr^{-1}.

3. Results

3.1. Nutrients Budgets

[23] The carbon and iron fluxes simulated by HAMOCC5 are displayed in Figure 1 for the euphotic zone (i.e., the upper 100 m of the ocean model). The iron budget is analyzed and discussed later in section 4.2. The annual net primary production for the global ocean is estimated to 42.6 Gt C yr^{-1}. This value falls within the range of recent

Table 3. Biological Parameter Values and Definitions[a]

Symbol	Unit	Value	Definition
		Phytoplankton Size-Classes	
a	day^{-1}	0.851	growth rate at 0°C
b		1.066	temperature sensitivity of growth
c	°C^{-1}	1	temperature dependence of growth
α	day^{-1}m^{2}W^{-1}	0.03	initial slope of P-I curve
k	m^2(W day)$^{-1}$	0.025	light extinction coefficient
I_0	W m^{-2}		irradiance at the surface
PAR		0.40	photosynthetically active radiation
K_N	μmol P L^{-1}	0.03/0.1	half-saturation constant for phosphate uptake
K_{Fe}	nmol Fe L^{-1}	0.02/0.12	half-saturation constant for iron uptake
K_{Si}^D	μmol Si L^{-1}	$0.8-8$	half-saturation constant for silicate uptake
P_{min}, D_{min}	μmol C L^{-1}	0.01	minimum phytoplankton concentration
K_P, K_D	μmol C L^{-1}	0.05	half-saturation constant for phytoplankton mortality
γ	day^{-1}	0.05/0.03	exudation rate of DOC
m_P	day^{-1}	0.008	specific mortality rate of nanophytoplankton
m_{min}	day^{-1}	0.01	minimum mortality rate of diatoms
m_{max}	day^{-1}	0.2	maximum mortality rate of diatoms
$\frac{Chl}{C}^{M}$	mg Chl (mg C)$^{-1}$	$\frac{1}{37}$	maximum $\frac{Chl}{C}$ ratio
$\frac{Chl}{C}^{M}$	mg Chl (mg C)$^{-1}$	$\frac{1}{90}$	minimum $\frac{Chl}{C}$ ratio
I_{par}^{max}	W m^{-2}	90	critical irradiance for photoadaptation
$\left(\frac{Si}{C}\right)^{av}$	μmol Si (μmol C)$^{-1}$	0.13	average $\frac{Si}{C}$ for diatoms
		Zooplankton Size-Classes	
ϵ		0.4	grazing efficiency
σ		0.15/0.25	egestion as faecal pellets
g	day^{-1}	14/3	maximum grazing rate
K_Z, K_M	μmol C L^{-1}	18	half-saturation constant for grazing
π_D, π_Z		0.5, 0.5	mesozooplankton feeding preferences
m	day^{-1}	0.01/0.05	specific mortality rate
γ	day^{-1}	0.25/0.05	excretion rate of DOC
ϵ_{can}		0.7	POC loss from higher trophic levels
Z_{min}, M_{min}	μmol C L^{-1}	0.01	minimum zooplankton concentration
		Organic Matter	
λ_{DOC}	day^{-1}	0.01	DOC remineralization rate
k_d	μmol P L^{-1}	0.3	half-saturation constant for DOC remineralization
r_{poc}	yr^{-1}	0.24	detrital breakdown rate
$R_{C:P}$		122:1	Redfield ratio of carbon to phosphate
		Iron	
$\frac{Fe}{C}^P$		4×10^{-6}	ratio of iron to carbon in zooplankton and nanophytoplankton
$\frac{Fe}{C}^{min}$		3×10^{-6}	minimum ratio of iron to carbon in diatoms
$\frac{Fe}{C}^{\star}$		17×10^{-6}	slope of the ratio of iron to carbon for diatoms
λ_{scav}^0	yr^{-1}	0.005	minimum scavenging rate of iron
$\lambda_{scav}^{\star}$	yr^{-1} (μmol C L)$^{-1}$	5×10^3	slope for the scavenging rate of iron

[a]When two values are given (separated by a /), the first value refers to the smallest size-class (nanophytoplankton or microzooplankton) and the second value refers to the largest size-class (diatoms or mesozooplankton).

estimates that give values between 36 and 57 Gt C yr^{-1} [*Longhurst et al.*, 1995; *Antoine et al.*, 1996; *Behrenfeld and Falkowski*, 1997]. Because of its coarse resolution, HAMOCC5 is not able to correctly resolve the coastal upwellings (for instance, the Peru upwelling), which are generally very productive zones [*Six and Maier-Reimer*, 1996]. Furthermore, mesoscale activity has been shown to have the potential to significantly enhance biological production [*Lévy et al.*, 1998; *McGillicuddy et al.*, 1998]. Thus, higher model resolution would certainly increase the predicted primary production.

[24] About one fifth of the predicted net primary production is due to diatoms. Estimates of the contribution of diatoms to global primary production are scarce and rather uncertain. *Nelson et al.* [1995] suggest that diatoms may be responsible for up to 40% of the total primary production for the global ocean, which is about twice as much as what HAMOCC5 simulates. However, in their budget, they assumed that diatoms represent about 35% of the phytoplankton standing stock in oligotrophic areas. Observations in the equatorial Pacific ocean, in the North Pacific subtropical gyre and in the Atlantic ocean show that diatoms contribution is generally less than 10% of the total phytoplankton biomass [e.g., *Scharek et al.*, 1999; *Belviso et al.*, 2001]. Furthermore, in the Southern Ocean, measurements of the diatoms relative abundance are generally below 50%, except in the Polar Front Zone and along the Antarctic Coast, a significantly lower value than the 75% assumed by *Nelson et al.* [1995] [e.g., *Fiala et al.*, 1998; *Bracher et al.*, 1999]. Thus, the estimate of *Nelson et al.* [1995] may be an upper limit of the diatoms contribution to the global net primary production. An older study by *Malone* [1980] suggests that about 80% of the primary production in oceanic waters of equatorial and temperate regions is related

to nanophytoplankton. Furthermore, the modeling study by *Moore et al.* [2002a] found that diatoms represent about 24% of the global primary production, a value close to ours.

[25] The model predicts that 10.6 Gt C yr^{-1} are exported below the euphotic zone. About 85% of this flux is related to the vertical sedimentation of particles. The remainder is mostly due to vertical advection and mixing of dissolved organic materials, especially in the high latitudes where convective mixing is intense. Estimating the contribution of the different living compartments to the export production is only partly feasible in the model, as a substantial fraction of this export is due to dissolved organic matter, which is not differentiated according to its origin. However, if we only consider the amount of carbon exported as POC, the "large cells loop" (diatoms and mesozooplankton) represents 55% of the 9.2 Gt C yr^{-1} that sink out of the euphotic zone, but only 20% of the net primary production. Thus for this loop, the e-ratio (defined as the ratio of the export production to the primary production) equals 0.61, which is typical of the Southern Ocean and of spring blooms in high latitudes where diatoms dominate [e.g., *Semeneh et al.*, 1998]. For the small size classes (microzooplankton and nanophytoplankton), the e-ratio is much smaller, about 0.12. This value is typical of oligotrophic regions, like the subtropical gyres, where primary production is mostly sustained by regenerated production.

[26] For silicate, the model predicts a vertical export of biogenic silicate of 106 Tmol Si yr^{-1}. This value is close to the 120 ± 20 Tmol Si yr^{-1} estimated for the global open ocean [*Treguer et al.*, 1995]. The mean $\frac{Si}{C}$ for diatoms uptake as predicted by HAMOCC5 is thus 0.15, similar to the average 0.13 ± 0.05 estimated for the global ocean [*Nelson et al.*, 1995]. However, observations suggest that about 50% of the biogenic silica redissolves in the upper 100 m of the ocean [*Nelson et al.*, 1995]. Such redissolution is not taken into account in HAMOCC5. This means that the predicted silica export should be halved. Yet, the modeled distribution of surface silicate is in reasonable agreement with the observations (see Figure 5). Reducing the silica export would noticeably increase mean surface concentrations. Another means would be to increase diatoms production. However, such increase is not possible in HAMOCC5 as diatoms growth is already limited by nutrients availability. Thus, there seems to be an inconsistency between model predictions and the observations.

3.2. Surface Chlorophyll

[27] Figure 3 shows a comparison between modeled and SeaWiFS chlorophyll concentrations for May and November. The overall observed patterns are qualitatively and quantitatively reproduced by the model. Very low chlorophyll concentrations of less than 0.05 mg Chl m^{-3} are found in the oligotrophic subtropical gyres both in the model and in the observations. In HAMOCC3.1, concentrations were much higher than observed in these areas [*Six and Maier-Reimer*, 1996]. Most of the improvement in HAMOCC5 is due to the use of a variable $\frac{Chl}{C}$ ratio, which decreases to values around $\frac{1}{150}$ in the center of the subtropical gyres whereas in HAMOCC3.1, this ratio was kept constant to $\frac{1}{60}$. In the equatorial regions, both observed and simulated

chlorophyll concentrations are relatively modest around 0.2–0.25 mg Chl m^{-3}. In particular, the model is able to reproduce the quite low levels observed in the equatorial Pacific ocean, despite sufficient phosphate. Earlier versions of the model but also other global ocean carbon cycle models were overpredicting the phytoplankton biomass in this region by as much as three times when based on only phosphate or nitrate as a limiting nutrient [*Six and Maier-Reimer*, 1996; *Aumont et al.*, 2002].

[28] During the productive season, chlorophyll concentrations are high in the middle and high latitudes in each hemisphere. In the North Atlantic, the extent of the region where concentrations are higher than 0.6 mg Chl m^{-3} is underestimated by the model, especially in the western part of the basin. Month-by-month comparison with satellite data shows that high chlorophyll concentrations are observed in this area during the whole Spring whereas HAMOCC5 simulates a single strong pulse in April. A possible explanation for this deficiency might be the lack of a synoptic forcing. Occasional wind bursts in these regions deepen the mixed layer during short time periods and then partly replenish surface waters with nutrients. In the North Pacific Ocean, chlorophyll concentrations are much lower than in the Atlantic Ocean at similar latitudes and remain relatively constant all year round. These quite modest and constant chlorophyll concentrations are explained in models by the shallow winter mixed layers ensuring significant standing stocks of phytoplankton and zooplankton during winter months [*Six and Maier-Reimer*, 1996; *Aumont et al.*, 2002]. Modeled concentrations show the same behavior except in March, where values reach 1.2 mg Chl m^{-3}. Such a deficiency was already noticed in HAMOCC3.1 [*Six and Maier-Reimer*, 1996]. It may be explained by the approximation of *André* [1990] parameterization we made in HAMOCC5 that may not be appropriate in this region where the mixed layer depth is of the order of the euphotic zone depth.

[29] In the Southern Ocean, the model simulates a band of very high chlorophyll concentrations along the Antarctic coast. This bloom remains confined south of 60°S. Such an homogeneous feature in not present in satellite data, even if very high levels are observed at some places, mostly in the Ross and Weddell Seas. Northward, chlorophyll concentrations are much lower, generally below 0.3 mg Chl m^{-3} both in the observations and in the model. A noticeable exception in the observation is over the Patagonian Plateau which is not well captured by the model. Possible explanations to this observed feature may be an enhancement of phytoplankton growth by local mesoscale activity, iron fertilization by mineral dusts transported from Patagonia [*Duce and Tindale*, 1991], or an influence of the Antarctic Circumpolar Current (ACC) which becomes meridional in the Southwest Atlantic [*Sullivan et al.*, 1993]. According to the model results, the second explanation does not seem to hold as surface waters are not depleted in iron because of high atmospheric deposition (see Figure 5). In fact, comparison between observed and simulated nutrients concentrations (silicate and phosphate) supports the third possible mechanism (Figure 5). In particular, the Patagonian Plateau is characterized by high silicate concentration (above
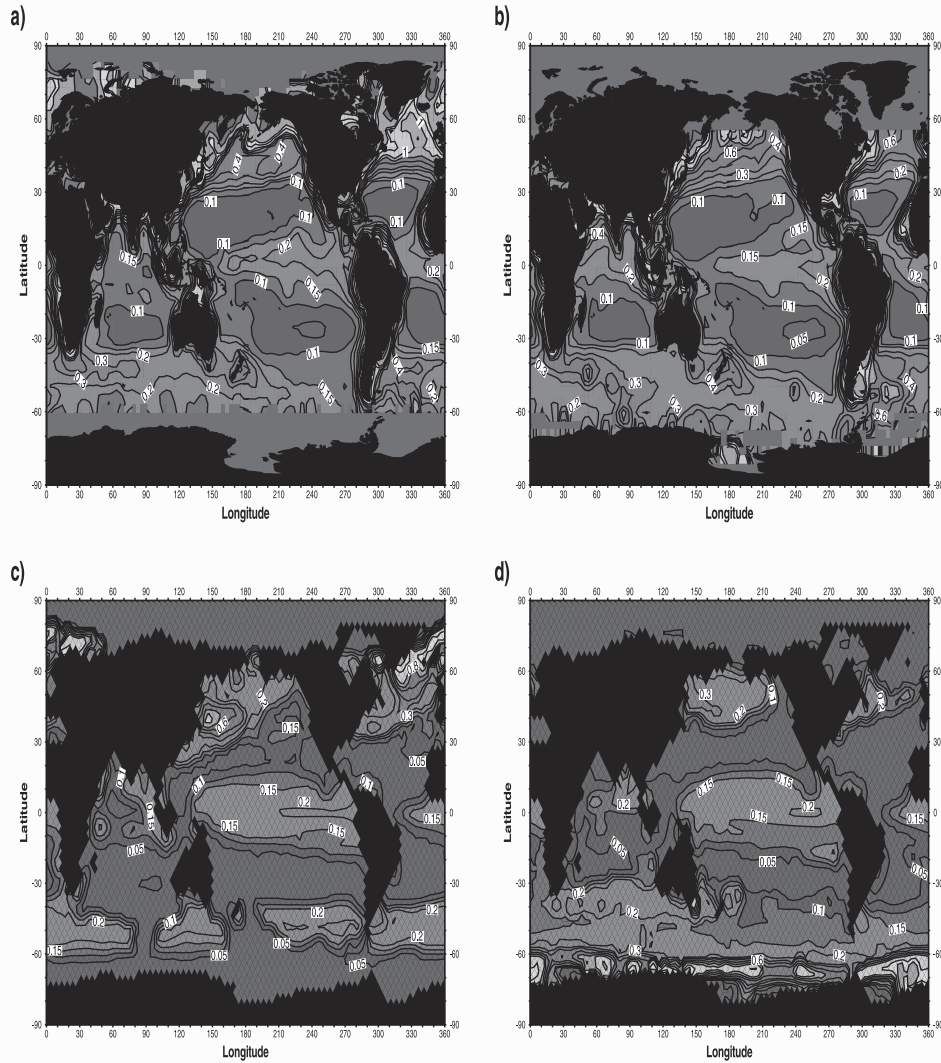
Figure 3. Monthly mean of the chlorophyll distribution (in mg Chl m^{-3}) from SeaWIFS and HAMOCC5 in May (a and c, respectively) and November (b and d, respectively). Satellite derived data have been interpolated onto a regular grid with a 3.5° horizontal resolution corresponding to the LSG model resolution. Isolines are at 0.05, 0.1, 0.15, 0.2, 0.3, 0.4, 0.6, 0.8, 1, 2, 4, and 6. See color version of this figure at back of this issue.

5 μmol L^{-1}) advected from the south by the ACC, a pattern which is not simulated by the model. However, an influence of mesoscale activity can not be excluded.

3.3. Diatoms Relative Abundance

[30] Figure 4 shows the relative contribution of diatoms to the total surface chlorophyll, also for May and November. Unfortunately, a global validation of this distribution is not yet feasible as it is for surface chlorophyll. However, there is an increasing number of in situ observations that give information on the taxonomic composition of phytoplankton biomass. To the first order, the relative abundance of diatoms follows the patterns of total chlorophyll. This result supports the common idea that large increase in phytoplankton biomass is generally related to diatoms blooms. Very low diatoms concentrations are

simulated in the oligotrophic regions with contribution of generally less than 10%. Such a low abundance has been observed at the HOT time series station in the North Pacific subtropical gyre [*Scharek et al.*, 1999]. In oligotrophic regions of the Atlantic ocean, higher values are predicted mostly around 20°N where high atmospheric deposition of iron originates from the Sahara. A meridional transect performed in the Atlantic ocean has reported such an increase at this latitude where diatoms relative contribution rises up to 30% whereas in the rest of the tropical Atlantic, diatoms are almost absent [*Maranon et al.*, 2000]. In these data, diatoms contribution also increases south of 30°S, especially during austral spring, to values up to 30%.

[31] In the well documented region of the equatorial Pacific ocean, modest diatom abundance is simulated by
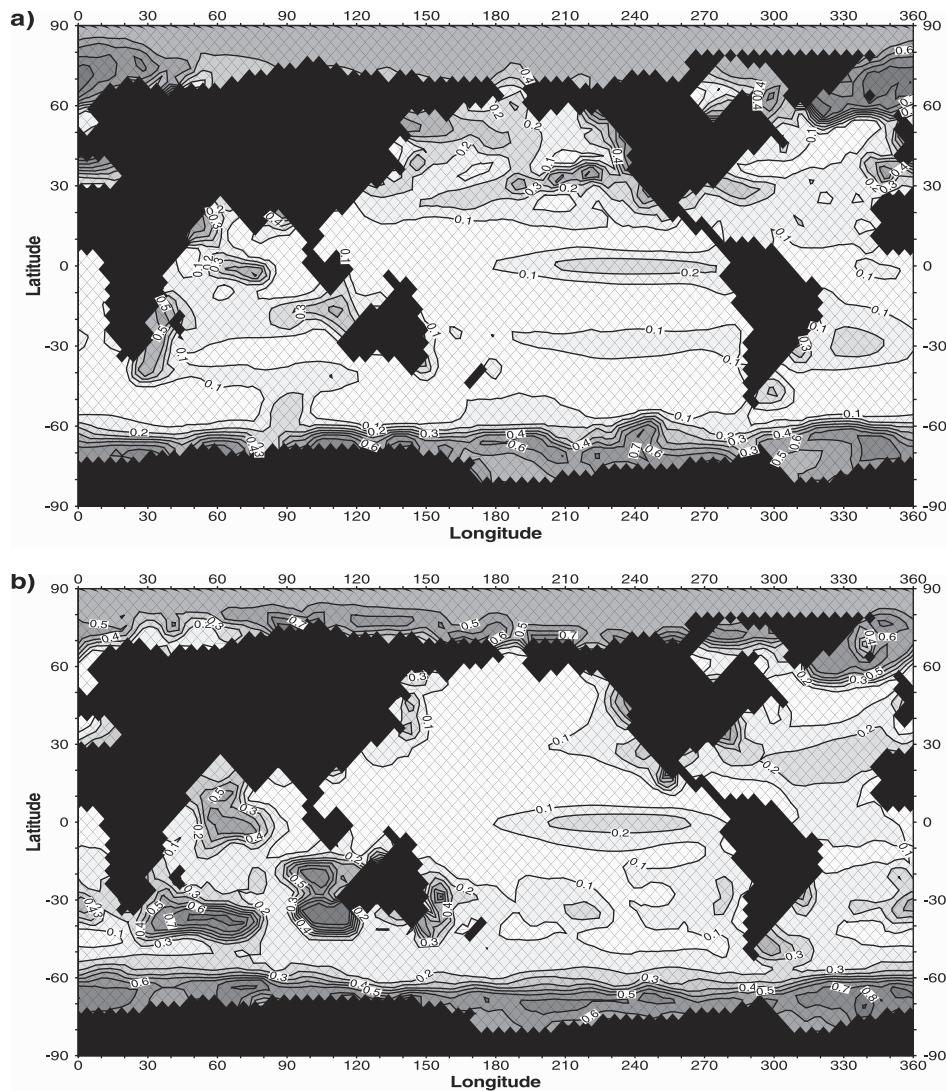
Figure 4. Monthly mean of the diatoms relative abundance as simulated by HAMOCC5 for (top) May and (bottom) November. Isolines are at 0.05, 0.1, 0.15, 0.2, and every 0.1 from 0.3 to 1.

the model. The maximum value, slightly more than 20%, is predicted in the central part of the basin, where the upwelling intensity is maximum bringing thus iron from the subsurface ocean. This maximum contribution is correlated to a maximum in chlorophyll concentration (see Figure 3). Data collected in 1992 during the EqPac cruises show that in this area, diatoms are almost absent (less than 10%), suggesting thus that the model overestimates their abundance [*Murray et al.*, 1994]. However, one should keep in mind that most of the cruises took place during and just after a warm anomaly associated with a strong reduction in the magnitude of the equatorial divergence. Some other estimates based on data collected during other years give much higher values of up to more than 30% [*Buck and Chavez*, 1994; *Blain et al.*, 1997].

[32] According to model results, diatoms constitute a large fraction of the total phytoplankton biomass during the phytoplankton bloom in the North Atlantic, even exceeding 80% in the Norwegian Sea. Observations generally show that diatoms dominate the phytoplankton biomass (around 50 to 60%), especially during the early stage of the bloom. Diatoms proportion tends to increase northward as suggested by the model [*Lochte et al.*, 1993]. After this phase, small flagellates become of increasing importance whereas the diatoms relative contribution declines to less than 20% [*Joint et al.*, 1993; *Savidge et al.*, 1995]. A similar drop in diatoms abundance can be observed in Figure 4 between 35 and 50°N, where the simulated bloom occurs in April. This decline is explained in the model by the exhaustion of silicate in surface waters. In the North Pacific Ocean, the situation is very different. Measurements made in the northeast subarctic Pacific Ocean show that the phytoplankton biomass is dominated by small autotrophic flagellates (from 50% to 70%) [*Boyd and Harrison*, 1999]. The larger size-class relative contribution is generally below 20% with significant interannual variations, close to the model predictions.
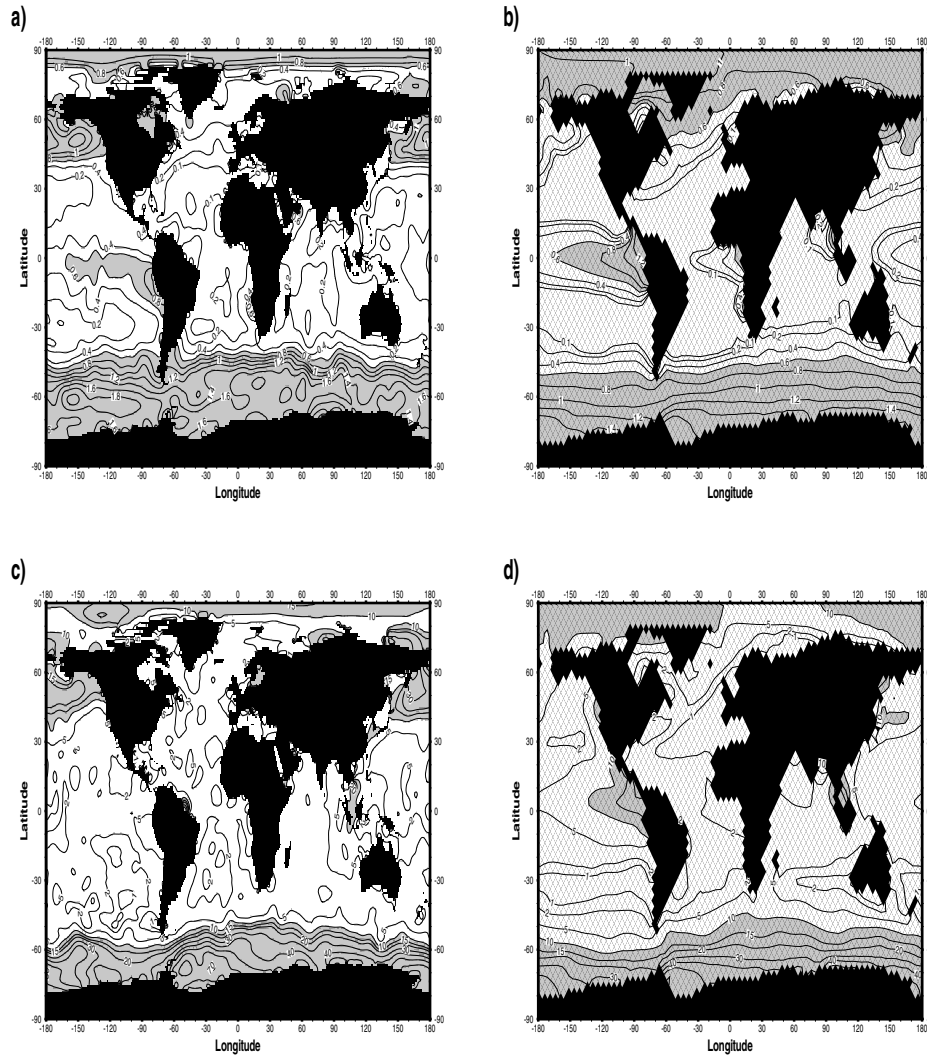
Figure 5. Mean surface phosphate concentration (in μmol P L^{-1}) from (a) the NODC database [*Conkright et al.*, 1994] and (b) HAMOCC5. Isolines are at 0.1 and every 0.2 from 0.2 to 2. Shaded area is above 0.6. Mean surface silicate concentration (in μmol Si L^{-1}) from (c) the NODC database [*Conkright et al.*, 1994] and (d) HAMOCC5. Isolines are at 1, 2, 5, 10, 15, and at every 10 from 20 to 70. Shaded area is above 10.

[33] The Southern Ocean can be roughly divided into two main domains from the model results. South of about 60°S, predicted phytoplankton biomass is dominated (above 50%) by diatoms. During austral spring and summer, diatoms relative abundance may even exceed 80%, mostly along the Antarctic coast. In situ measurements have also supported such a large contribution of diatoms, even if strong blooms of *Phaeocystis Antarctica* are common in well-mixed surface waters [*Wright and van den Enden*, 2000]. North of this 60°S limit, contribution from diatoms drops to usually less than 20%. A noticeable exception is the Indian sector of the Southern Ocean where diatoms are much more abundant. This localized maximum is due to enhanced atmospheric deposition of iron that is transported from Australia and Africa. Observations support the model predictions and generally show diatoms relative abundance below 10 to

20% north of 60°S [*de Baar et al.*, 1999]. However, transects performed across the Polar Front (around 55°S) indicate higher local chlorophyll concentrations with a significant contribution from diatoms. This local enhancement in a frontal region may be induced by the injection of nutrients, most presumably iron, from the subsurface due to strong mesoscale activity, even if lateral transport from continental shelves can not be excluded (at least in the Atlantic) [*de Baar et al.*, 1999]. Because of its coarse resolution, HAMOCC5 is not able to capture this localized maximum.

3.4. Nutrients Distribution

[34] Figure 5 present a comparison between simulated and observed phosphate and silicate concentrations at the surface on an annual mean basis. The simulated large-scale
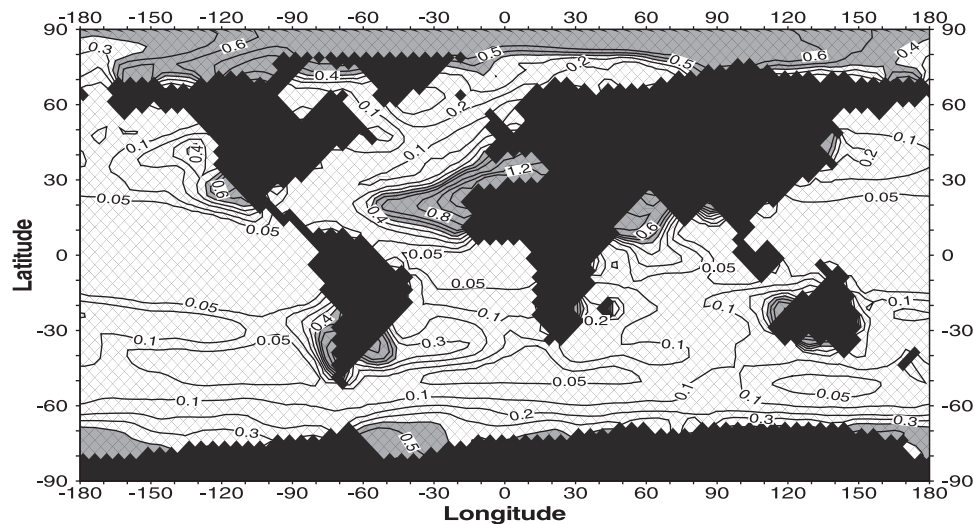
Figure 6. Annual mean surface concentration of Iron (in nM) from HAMOCC5. Isolines are at 0.05, 0.1, at every 0.1 from 0.1 to 0.6, and at every 0.2 from 0.6 to 1.2. Shaded areas denote concentrations above 0.4 nM.

patterns are in general agreement with the database constructed from observations [*Conkright et al.*, 1994]. In particular, relative to the previous model HAMOCC3.1, the phosphate concentration in the equatorial Pacific Ocean is in better agreement with the observations. The 0.5 μmol P L^{-1} isoline now stops at about 170°W instead of 150°E, thus closer to the observed 160°W. However, the phosphate distribution in this region is still nearly symmetrical about the equator whereas in the observation, highest concentrations are found south of the equator in the Peru upwelling. The too coarse resolution of the LSG model explains such a deficiency as the model is not able to properly resolve the coastal upwellings [*Toggweiler and Samuels*, 1993; *Aumont et al.*, 1999].

[35] The most prominent deficiency in the model is the too low phosphate and silicate concentrations in the North Pacific subpolar gyre. This problem seems to come from unrealistic representation of the dynamics by the LSG model which overestimates the stratification and/or underestimates the vertical pumping of nutrients to the surface. In addition, the occurrence in the model of a faulty moderate bloom of nanophytoplankton in March enhances the phosphate depletion. However, the latter point should not be dominant as silicate distribution also exhibits much too low values in this region. The predicted relative abundance of diatoms seems to be in the range of the observed values (see section 3.3). Furthermore, the average $\frac{Si}{C}$ simulated in this region is between 0.13 and 0.3, values that are typical of the subarctic Pacific Ocean [*Wheehler*, 1993]. This problematic representation of the ocean dynamics in the North Pacific subpolar gyre appears to be typical of global coarse resolution models [*Six and Maier-Reimer*, 1996].

[36] Figure 6 displays the annual mean surface distribution of iron predicted by HAMOCC5. Unfortunately, despite the increasing number of iron data, a global validation of the model prediction similar to what we did for

silicate and phosphate is still not feasible. The model simulates large horizontal gradient of iron at the surface. Largest values, that may exceed 1 nM, are predicted in regions of intense dust deposition, mainly the Arabian Sea and the eastern subtropical North Atlantic Ocean. However, these large iron concentrations are not advected far away from these areas, as scavenging and biological production remove iron quickly from surface waters. A cruise performed recently across the Atlantic Ocean from about 50°N to about 40°S has found iron concentrations of up to 0.4 nM near the Canary Islands whereas south of about 10°N, iron levels drop below 0.1 nM (S. Blain, personal communication, 2000). Relatively large iron concentrations are also simulated in the high latitudes of the North Atlantic Ocean and along the Antarctic Coast as a result of deep winter mixing. In the Southern Ocean, observations have shown such an increase toward the Antarctic Coast where concentrations of about 0.6 nM have been reported [*Sohrin et al.*, 2000]. In the rest of the ocean, predicted iron concentrations are quite low, typically below 0.1 nM.

[37] The vertical iron structure predicted by the model is compared to observations at six stations selected from the database released by *Johnson et al.* [1997] (Figure 7). In the top thousand meters of the ocean, the predicted vertical gradient of iron is systematically overestimated. A possible explanation for this flaw could be a too shallow release of iron by remineralization of the organic matter. However, a comparison of the phosphate and silicate profiles at the same stations shows a similar problem. With a different biogeochemical model but the same ocean model (except for the vertical resolution), *Archer and Johnson* [2000] also noticed this bias in the thermocline. In fact, such a deficiency highlights the limits of the coarse resolution ocean circulation model, especially because the vertical diffusivity in the thermocline is too strong. However, as given by *Archer and Johnson* [2000], the ratio of iron to phosphate in the subsurface waters is not significantly different from the
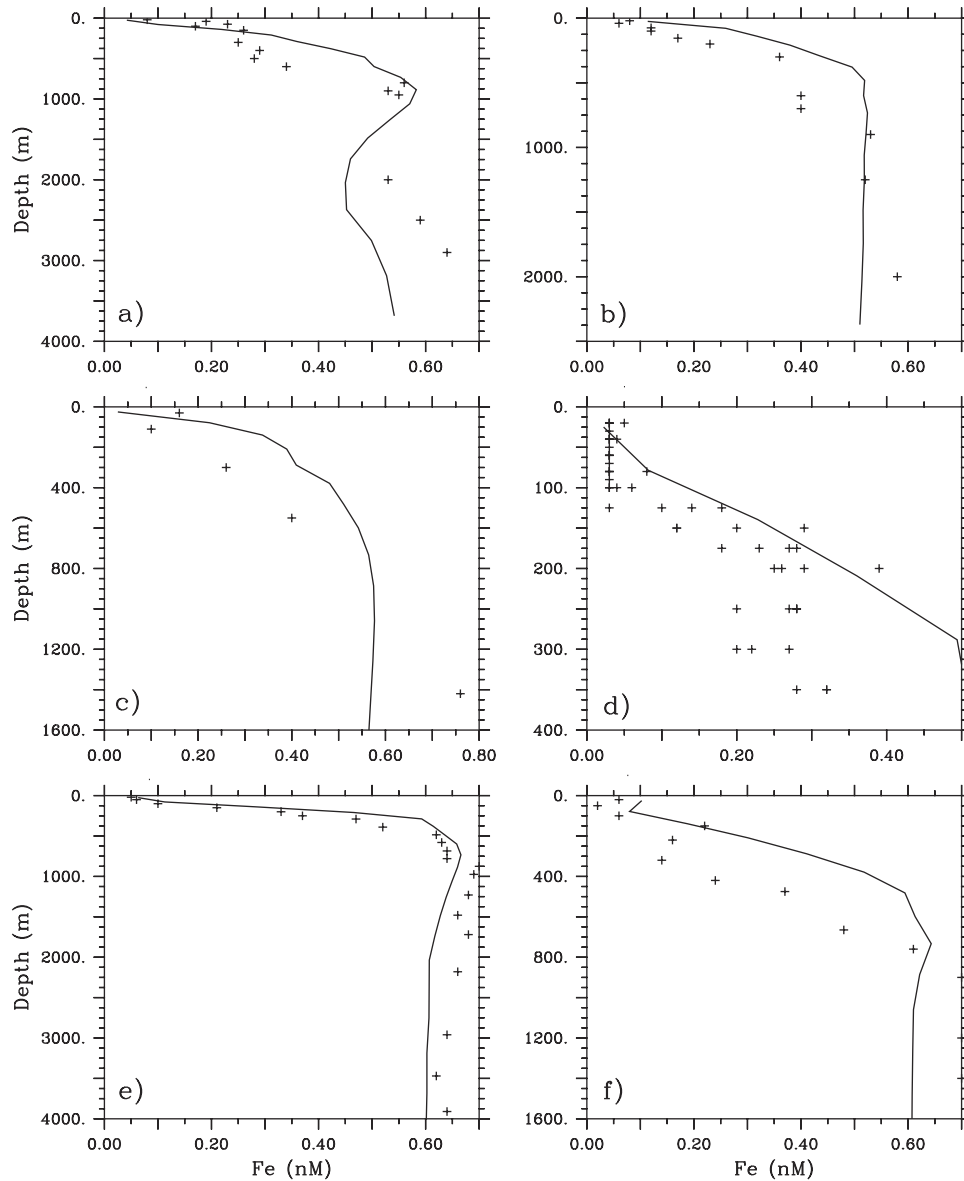
Figure 7. Vertical profiles of iron (in nM) from data (pluses) and from HAMOCC5 (solid line) at (a) NABE 47N (47°N, 20°W) in May, (b) NABE 59N (59°N, 20°W) in June, (c) Drake Passage (61°S, 60°W) in March, (d) Eqpac (0°N, 140°W) in Spring-Fall, (e) VertexVII station 7 (50°N, 145°W) in August, and (f) Vertex VI station T3 (31°N, 146°W) in September.

observations. The latter ratio determines which of these nutrients is the most limiting for phytoplankton growth.

4. Discussion

4.1. Colimitations by Fe, P, and Si

[38] The validation of HAMOCC5 with available observations has shown that this model is able to correctly simulate the main characteristics of the ocean biogeochemistry. This suggests that the main processes controlling the biological production are correctly resolved, given the deficiencies in the ocean dynamics simulated by coarse-resolution models. In particular, the model is able to reproduce the HNLC areas, except for the subarctic North

Pacific Ocean, where an unrealistic modeled ocean dynamics leads to erroneous results. Thus, using HAMOCC5, one may try to determine on the global scale the regional and temporal distribution of the limitations by the different modeled limiting nutrients.

[39] Figure 8a shows the temporal occurrence of the limitations by the three different nutrients over the global ocean for nanophytoplankton. As nanophytoplankton does not need silicate to grow, this nutrient is of course never limiting. Three main biogeochemical regimes can be distinguished from this distribution of the nutrients limitations. First, in the oligotrophic regions, mainly the subtropical gyres, nanophytoplankton growth is limited by phosphate. As the model does not distinguish between nitrate and
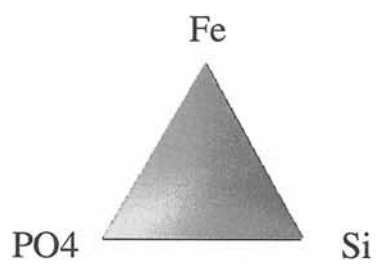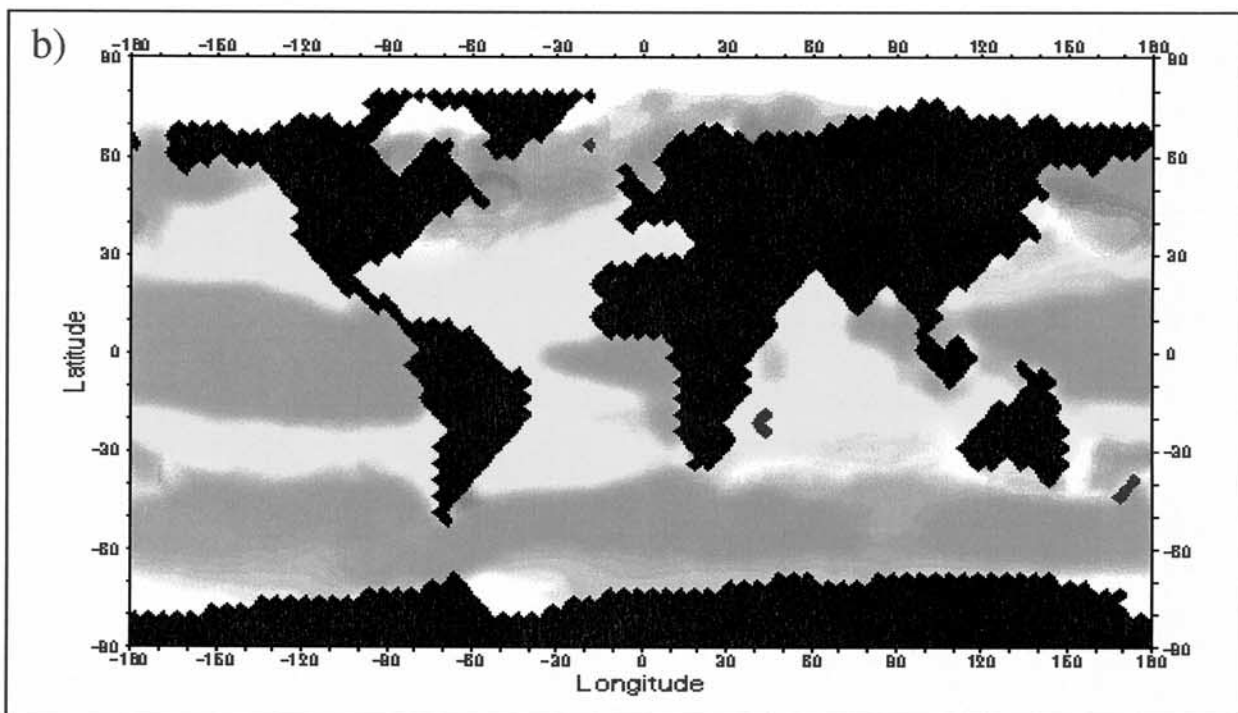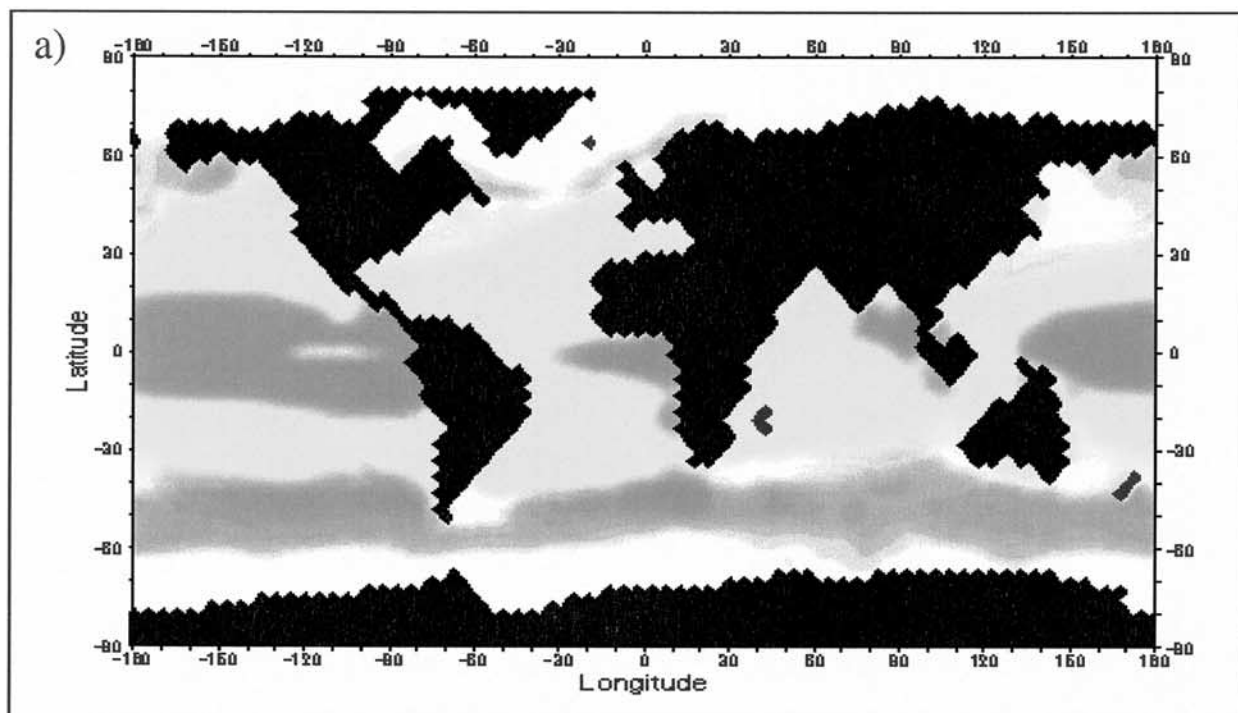
phosphate, it is not possible to infer from model results which one of these two nutrients is the most limiting. Second, in the main HNLC areas, i.e., the equatorial Pacific ocean, the Southern Ocean and the subarctic North Pacific Ocean, iron is limiting nanophytoplankton growth. Finally, in the high latitudes, generally poleward of 60°, light limitation becomes dominant. This latitudinal limit corresponds approximately to the maximal extent of the sea ice cover. However, light limitation is also acting equatorward of this limit, in the North Atlantic, in the western part of the North Pacific and in the Indian sector of the Southern Ocean where the predicted mixed layer depth is very deep during winter time.

[40] Thus, for nanophytoplankton, the regional distribution of the nutrients limitations agrees well with the now well-accepted theory that HNLC areas are explained by iron limitation. Light limitation plays also an important role, especially in the Southern Ocean. However, the magnitude of the iron limitation in the HNLC areas, which is given by the value of the Michaelis-Menten function, is generally significantly less severe than the phosphate limitation in the traditional oligotrophic regions. More than the lack of iron, grazing pressure exerted by microzooplankton is mainly preventing nanophytoplankton from reaching important concentrations. Almost everywhere, except in the very oligotrophic parts of the subtropical gyres (their center), nanophytoplankton growth rate is balanced by loss rate due to microzooplankton grazing throughout the year (Figure 9). Consequently, nanophytoplankton biomass is relatively constant to about 0.1–0.2 mg Chl m^{-3} with only moderate seasonal variations, especially compared to diatoms. This tight coupling between nanophytoplankton and microzooplankton is explained by similar doubling rates and is a general feature of oligotrophic and HNLC systems [*Verity et al.*, 1996; *Landry et al.*, 2000].

[41] The largest chlorophyll concentrations associated with the nanophytoplankton size class are reached in the high latitudes with typical values around 1 mg Chl m^{-3}. This has to be compared with diatoms blooms which often exceed 2 mg Chl m^{-3} in HAMOCC5. This relatively modest seasonal increase in nanophytoplankton biomass is consistent with observations [*Gifford et al.*, 1995]. However, these values are yet above those found at low latitudes where typical nanophytoplankton concentrations are below 0.3 mg Chl m^{-3}. Thus, some uncoupling between nanophytoplankton growth and grazing pressure by microzooplankton is not impossible, at least in high latitudes after deep winter mixing.

[42] Figure 8b shows the regional distribution of nutrient colimitations for diatoms predicted by HAMOCC5. The general patterns are similar to those for nanophytoplankton with the exception of the North Atlantic and some parts of the frontal zones in the Southern Ocean where silicate limitation is dominating. Nutrients limitation is always stronger for diatoms than for nanophytoplankton. It reflects the lower affinity diatoms have for nutrients because of their lower surface/volume ratio which is represented in HAMOCC5 by higher half-saturation constants (see Table 3) [*Sakshaug and Holm-Hansen*, 1977]. This stronger control by nutrients availability explains the small contribution of diatoms to the total phytoplankton biomass in oligotrophic areas with small seasonal variability (oligotrophic in the sense that one nutrient is missing, either silicate, phosphate or iron).

[43] Unlike nanophytoplankton, diatoms may undergo strong increase in their biomass. The main regions where those blooms are observed are the North Atlantic Ocean north of 40°N [*Ducklow et al.*, 1993] and some parts of the Southern Ocean, especially in the marginal ice zones [*Mitchell et al.*, 1991]. During these sudden explosions of phytoplankton biomass, which frequently exceeds 2 mg Chl m^{-3}, phytoplankton assemblages are often, but not always, dominated by diatoms [e.g., *Joint et al.*, 1993; *Lochte et al.*, 1993]. The model explains the dominance of the larger species during these blooms by size-differential grazing. Because of their rapid doubling rates, microzooplankton keeps in control nanophytoplankton when favorable conditions are met. On the other hand, because of their lower growth rates, mesozooplankton is not able to control the development of large phytoplankton (see Figure 9). Such an inefficient grazing pressure by mesozooplankton on diatoms has been observed in situ in the North Atlantic Ocean [*Morales et al.*, 1991; *Dam et al.*, 1993] and in the Southern Ocean [*Froneman et al.*, 2000]. Furthermore, a possible control by the rapidly growing microzooplankton is not likely to occur as they primarily graze on small phytoplankton [*Dagg*, 1993; *Gifford et al.*, 1995]. Such a differential size-grazing pressure on phytoplankton has been also proposed to explain the diatoms-dominated increase in phytoplankton biomass during the IRONEX II experiment in the eastern equatorial Pacific [*Landry et al.*, 2000].

[44] In the North Atlantic, the termination of the strong spring bloom of diatoms is explained in HAMOCC5 by silicate deficiency, as shown in Figure 8b. Such a control of the magnitude and the duration of the diatom bloom by silicate availability has been confirmed by in situ observations which show that silicate is the first macro-nutrients to

Figure 8. (opposite) Nutrient colimitations of (a) nanophytoplankton and (b) diatoms by the three modeled nutrients. The colors denote the temporal occurrence of the limitation by the different nutrients. Thus a full yellow color means that the ecosystem is limited by phosphate all year long. A mix of two different colors means that over the year, the ecosystem is limited by two different nutrients. The limiting nutrient is computed from $L_{P,D}$ (see Table 2). The intensity of the colors is modulated to give extra-information both on the magnitude of the nutrient limitations and on the light limitation. Paler colors mean that during part of the year, biological production is either not limited by nutrients or is light limited. Phytoplankton growth is considered to be light limited when the convective depth is deeper than 100 m. Furthermore, the three modeled nutrients are considered not to be limiting when the Michaelis-Menten function is larger than 2/3. These maps have been computed from monthly mean fields. See color version of this figure at back of this issue.
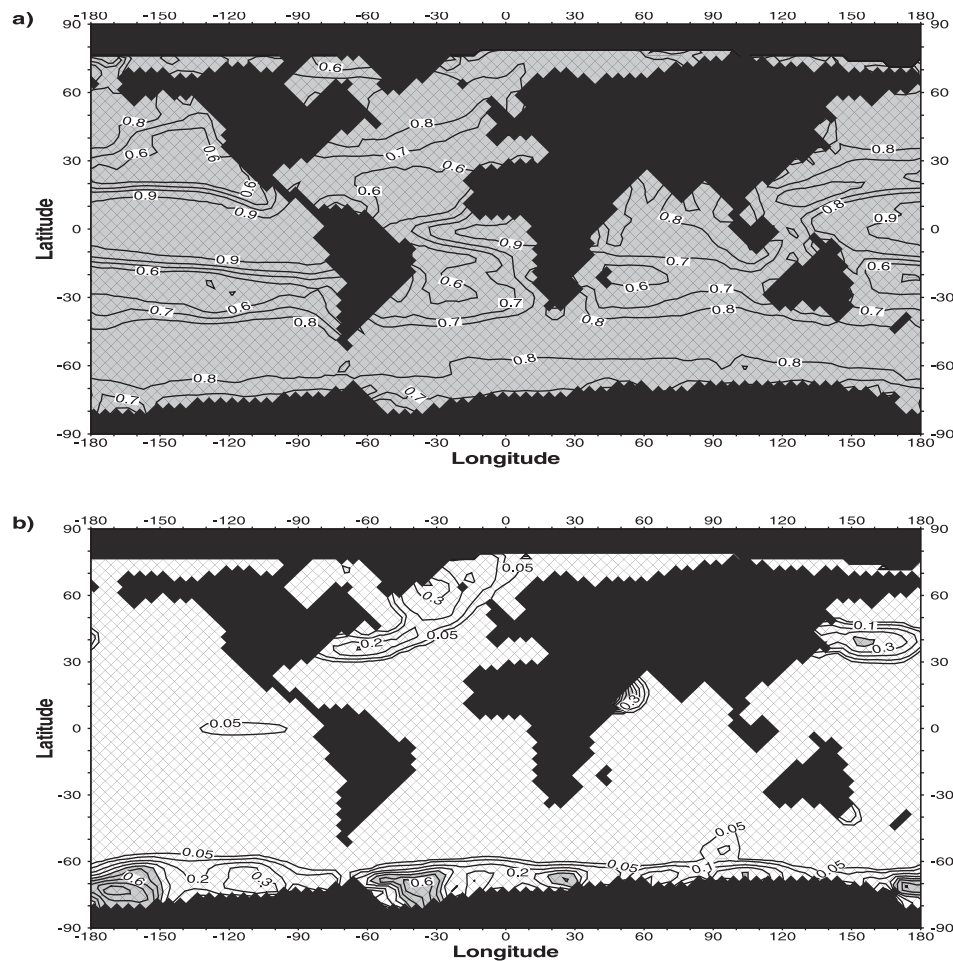
Figure 9. Annual mean amount of primary productivity lost by grazing for (a) nanophytoplankton and (b) diatoms. Shaded areas denote values higher than 40%. Isolines are at 0.05 and every 0.1 from 0.1 to 1.

be exhausted from the euphotic zone. Consequently, the phytoplankton community undergoes a shift from diatoms to flagellates dominant species [*Sieracki et al.*, 1993; *Dale et al.*, 1999]. Such a preferential uptake of silicate over that of other macro-nutrients is also observed in the Southern Ocean across the Polar Frontal Zone [*Treguer and van Bennekom*, 1991; *Dafner and Mordasova*, 1994] as well as it is predicted by the model (Figure 5).

[45] Several explanations have been proposed to explain this more severe depletion in silicic acid relative to phosphate and nitrate: low dissolution rate of biogenic silica, a preferential ammonium uptake and iron limitation which has a stronger impact on phosphate and nitrate uptake rate [*Kamykowski and Zentara*, 1989; *Franck et al.*, 2000]. Except for the potential effect of ammonium which is not explicitly modeled, the model is consistent with these explanations. In the North Atlantic, about 50% of the phosphate used by diatoms is recycled within the euphotic zone whereas almost all the biogenic silica is exported into the deep ocean. There is only a small impact of iron just at the termination of the bloom as this nutrient is generally sufficient in this region due to high dust deposition and intense winter mixing. In the Southern Ocean, the role of

iron is more critical. The more severe reduction in phosphate assimilation by iron deficiency, which results in high Si/C ratios in diatoms, increases the overconsumption of silicate over phosphate. However, except near Australia, silicate is not limiting diatom growth in the Southern Ocean in HAMOCC5. Such result is not consistent with observations which show evidence of silicate limitation on the north side of the Polar Front [*Jacques*, 1983; *Boyd et al.*, 1999]. An iron maximum is often observed in the Polar Front, probably due to local enhancement of vertical supply by mesoscale activity [*de Baar et al.*, 1995, 1999]. Because of its coarse resolution, such maximum can not be resolved by HAMOCC5, which simulates an overall iron limitation for diatoms growth instead of an expected silicon limitation.

4.2. Iron Budget

[46] About 20% of the surface ocean is characterized by typical HNLC conditions. Our model results support the now well accepted hypothesis that biological production is generally limited in these areas by iron availability, despite light and silicon may also be important, especially in the Southern Ocean. Such a limitation suggests that over large regions of the global ocean, the supply of iron is controlling

the magnitude and the variability of the ocean primary production. Furthermore, because diatoms are more sensitive to iron levels than smaller phytoplankton, the rate of iron supply is critical not only for the primary production but also for the efficiency of the biological pump to export carbon to the deep ocean. Thus, an increase in the iron supply would lead to a larger export production and a more phosphate-controlled system, until a limit is reached set by the total supply of phosphate to the euphotic zone [*Archer and Johnson*, 2000].

[47] Using HAMOCC5, we have estimated the iron budget in the euphotic zone (the top 100 m of the ocean model, Figure 1). 18×10^9 mol Fe yr^{-1} are assimilated by phytoplankton to sustain primary productivity. Thus, for the global ocean, the average $\frac{Fe}{C}$ for phytoplankton is estimated to about 5.1×10^{-6} mol.mol^{-1} by HAMOCC5. Using a model and observations, *Fung et al.* [2000] have estimated the global assimilation of Fe to be about 12×10^9 Fe yr^{-1} for the open ocean. This substantially lower value is mostly due to their use of a smaller $\frac{Fe}{C}$ for phytoplanktonic cells, on average about 4×10^{-6} mol.mol^{-1}. This significant difference between the two estimates highlights the uncertainties on the values taken by this ratio.

[48] From the global budget for iron displayed in Figure 1, one would be tempted to infer the relative contribution of atmospheric deposition and ocean transport to sustain the phytoplankton demand for iron. However, the net injection of iron to the top 100 m of the ocean from the subsurface (3.5×10^9 Fe yr^{-1} according to HAMOCC5) may underestimate the relative role of the ocean transport by including a downward transport of atmospheric iron. To correct for that potential vertical transport of atmospheric iron, we have performed a new simulation. In that additional run, dissolved iron has been split into two components corresponding to the two different sources. Both components experienced the same processes except that ocean iron also includes local regeneration whereas atmospheric iron is only supplied from aeolian deposition. According to that experiment, 0.15×10^9 mol Fe yr^{-1} of atmospheric iron is transported downward into the deep ocean. Consequently, 3.65×10^9 mol Fe yr^{-1} of the new iron taken up by phytoplankton is supplied by the ocean transport. The latter supplies about 75% of the new iron to the euphotic zone, instead of the 70% deduced from Figure 1.

[49] The prediction of HAMOCC5 for the relative contribution of the two considered sources of new iron is within the range (70–80%) given by *Archer and Johnson* [2000] and *Moore et al.* [2002a]. The net upward input of new iron predicted by HAMOCC5, 3.65×10^9 mol Fe yr^{-1}, is also very close to the about 3.4×10^9 mol Fe yr^{-1} found by *Archer and Johnson* [2000]. Comparison with the budget proposed by *Moore et al.* [2002a] is rather difficult to perform as their estimate is computed for the surface mixed layer which may be either much deeper or much shallower than the 100m we chose here. However, all the model-based studies suggest that the ocean plays a dominant role in the iron budget. On the other hand, our estimate is about six times larger than the 0.7×10^9 mol Fe yr^{-1} computed by *Fung et al.* [2000]. Thus, why is there such a difference

between the fully model-based approaches (like in our study) and the data-based estimate of *Fung et al.* [2000]?

[50] Most of the difference between the model-based and data-based approaches is explained by the magnitude of the vertical supply of new iron by the ocean dynamics. The regional distribution of this vertical supply as predicted by HAMOCC5 is displayed in Figure 10. This transport includes advection, diffusion and convection. It may be directly compared to Plate 1 of *Fung et al.* [2000]. HAMOCC5 predicts a total upward transport of new iron of 4.5×10^9 mol Fe yr^{-1} into the top 100 m of the ocean. The downward transport of iron is not negligible and is estimated to 1×10^9 mol Fe yr^{-1} by HAMOCC5, of which 15% is originating from the atmosphere (see above). Thus, about 17% of the total new iron supplied by the ocean and the atmosphere is transported out of the euphotic zone by the ocean circulation. For comparison, the ratio of the downward to upward transport is about 40% for phosphate. Thus, the iron uptake is much more efficient than the phosphate uptake.

[51] Our predicted vertical supply of iron differs from that of *Fung et al.* [2000] mostly in the high latitudes and in the equatorial Pacific ocean. In the high latitudes, HAMOCC5 predicts a vertical input of new iron that often exceeds 20 μmol Fe m^{-2} yr^{-1} whereas in work by *Fung et al.* [2000], it is generally below 10 μmol Fe m^{-2} yr^{-1} (except for some areas near Iceland in the North Atlantic). In those regions, more than half of the transport simulated by HAMOCC5 is related to winter convection and diffusion. The treatment of winter mixing is very different in the two studies. In HAMOCC5, a one pass convective adjustment is applied whereas in work by *Fung et al.* [2000] a vertical diffusivity coefficient of at most 1 cm^2 s^{-1} is prescribed. The latter approach induces a much less vigorous vertical mixing than the convective algorithm used in HAMOCC5. Numerical experiments performed with explicit parameterizations of the oceanic vertical mixing lead to typical vertical diffusivity coefficients that are several orders of magnitudes larger than 1 cm^2 s^{-1} [*Gaspar et al.*, 1990]. Consequently, the data-based study may have largely underestimated the contribution of vertical mixing in the high latitudes to the global vertical input of new iron in the photic zone from the subsurface.

[52] In HAMOCC5, convection brings to the surface about 1.1×10^9 mol Fe yr^{-1}, about 60% more than the total vertical supply of new iron from the deep ocean estimated by *Fung et al.* [2000]. *Moore et al.* [2002a] also found that vertical mixing in the high latitudes contributed strongly to the injection of new iron to the surface. In fact, they found an input of 13×10^9 mol Fe yr^{-1}, that is more than 10 times our estimate. The difference is most likely explained by the vertical extent of the domain on which the iron budgets are computed. [*Moore et al.*, 2002a] estimated the inputs of iron for the complete surface mixed layer, which may be more than 500 m deep, whereas we restricted our computation to the top 100 m of the ocean. Furthermore, they have artificially increased the subsurface iron concentrations in the North Atlantic, a region where winter mixing is very intense.
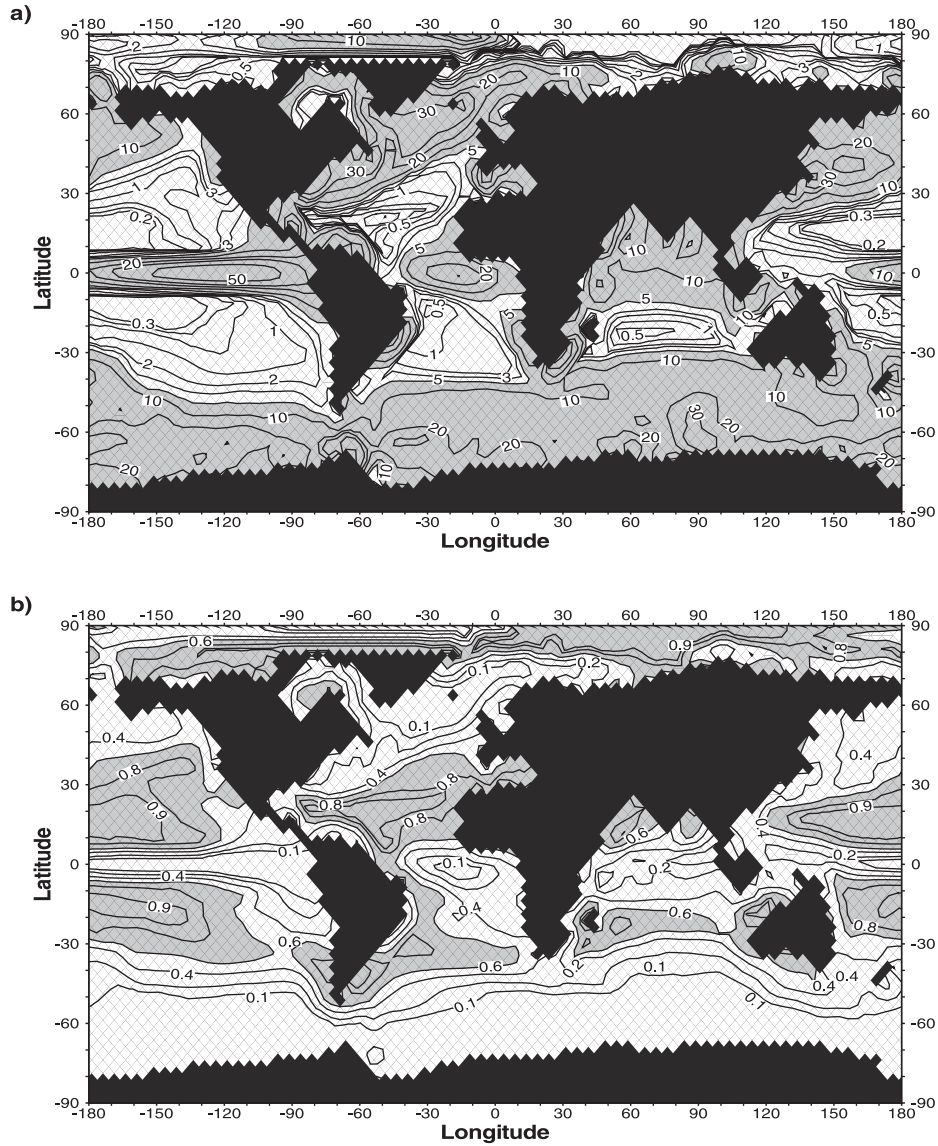
Figure 10. Annual mean global distribution of (a) total dissolved iron supplied into the top 100 m of the ocean by advection, diffusion and convection as predicted by HAMOCC5 and (b) the ratio of atmospheric fluxes of new iron to the total supply of new iron by the ocean and the atmosphere into the top 100 m of the ocean. Unit of Figure 10a is μmol Fe yr^{-1}.

[53] In the equatorial Pacific ocean, our estimate and that of *Fung et al.* [2000] of the upwelled/entrained supply of new iron diverge to a large degree. In HAMOCC5, the upward flux exceed 50 μmol Fe m^{-2} yr^{-1} in the central basin whereas according to *Fung et al.* [2000], this flux is about 5 times lower. For instance, at 140°W, *Fung et al.* [2000] estimated a flux of about 12 μmol Fe m^{-2} yr^{-1} at the base of the photic zone while HAMOCC5 predicts an input of 68 μmol Fe m^{-2} yr^{-1}. At this location, *Gordon et al.* [1997] have constructed a simple one-dimensional model based on observations to compute iron fluxes into the euphotic zone. They estimated the upward flux of iron to 44 ± 13 μmol Fe m^{-2} yr^{-1} at 120 m. This value is about 40% lower than what HAMOCC5 predicted. On the other

hand, according to *Gordon et al.* [1997], *Fung et al.* [2000] may have underestimated this flux by a factor of 4.

[54] We believe that our estimate probably represents an upper limit. First, the modeled vertical gradients of dissolved iron are generally overestimated in the thermocline (Figure 7). Thus, subsurface iron concentrations are too elevated compared to observations. Such deficiency may partly explain why our estimate is significantly larger than that of *Gordon et al.* [1997] in the equatorial Pacific. Second, predicted winter convection may be too intense in the Southern Ocean. The LSG model simulates along the Antarctic Coast convection that typically reaches the bottom of the ocean during winter time whereas observations confine such a deep convection to localized

Table 4. Results of Sensitivity Analysis[a]

Experiment	Parameter Value	Total Primary Production	Percent Diatoms	Export Production	BSi Export
Standard		42.6	19	9.2	106
Constant scavenging rate	0.005	41.4	24	9.6	108
Constant	5×10^{-6}	40.9	29	10	112
Light independent		41.6	22	9.4	109
Increased iron solubility	0.1	39.5	33	10.2	112
Constant	0.13	42.4	20	9.3	85
Constant K_{Si}^D	1	42.5	20	9.3	108

[a]All numbers are globally integrated annual mean values. Primary production and export production are in Gt C yr^{-1}. Biogenic Silica export (BSi export) is in Tmol Si^{-1}. % Diatoms refers to the relative contribution of diatoms to the total primary production. Export is referenced to the bottom of the productive zone (100 m).

areas of the Antarctic Ocean, mainly the Ross and Weddell Seas [*Killworth*, 1983]. On the other hand, the estimate proposed by *Fung et al.* [2000] might be a lower limit as (1) vertical diffusion coefficients are too low in the high latitudes and (2) comparison with the computation by *Gordon et al.* [1997] suggests that their upward flux is too small in the equatorial Pacific. Thus, we propose $0.7-4.5 \times 10^9$ mol Fe yr^{-1} as a range for the upwelled/entrained flux of iron into the euphotic zone (i.e. the top 100 m of the ocean). This sets the relative contribution of the ocean to 33–75% if only the ocean and the atmosphere are considered as potential sources of new iron for the marine primary productivity and if a 1% solubility is assumed for depositing dust. The ocean supplies then a large proportion of the phytoplankton demand for iron.

[55] Quantifying the uncertainties associated with our budget is rather difficult. These uncertainties have been already identified by *Fung et al.* [2000] in their conclusion. The major problem comes from our ignorance of the iron biogeochemistry in the ocean and from the poor coverage of iron measurements. For instance, the magnitude and the regional patterns of iron deposition are still largely uncertain as illustrated by the comparison from different estimates based on atmospheric models or data [see *Archer and Johnson*, 2000, Figure 3]. Furthermore, the magnitude of the delivery of iron from coastal zones has been proved to be important even in the open ocean [*Blain et al.*, 2001]. That input has been ignored up to now in global studies of the iron cycle, including our work. Another uncertainty is the coarse spatial and temporal resolution of the world ocean models which prevents them from correctly representing small-scale dynamics structures like mesoscale eddies or coastal upwellings. Several case or regional studies have shown that intense vertical velocities associated with mesoscale meanders and eddies significantly enhance the vertical supply of nutrients and then the biological activity [e.g., *Lévy et al.*, 1998; *Oschlies and Garçon*, 1998; *McGillicuddy et al.*, 1998]. Such a study is still to be done on the global scale.

4.3. Sensitivity Experiments

[56] The model solution we present here of course depends highly on the parameterizations we assumed for modeling biological processes and on the set of parameters we assigned to those parameterizations. These choices we made for HAMOCC5 are based mostly on the literature.

However, some preliminary simulations were necessary to adjust the parameters in order to achieve a reasonable solution. It would be interesting to understand how sensitive that solution is to our choices. However, a complete sensitivity study is out of range considering the very large computing cost the numerous necessary runs to equilibrium would demand. Furthermore, such analyses on parameter dependence have been already performed with 1-D biological models which are conceptually similar to HAMOCC5 [*Pondaven et al.*, 1999; *Leonard et al.*, 1999]. These studies show that the models are most sensitive to phytoplankton and zooplankton closure terms, mainly the grazing and mortality rates.

[57] We have focused our sensitivity study on the parameterizations we introduced to model the iron and the silicon cycles and their effects on biological production. The tests we performed are summarized in Table 4. The model was most sensitive to iron parameterizations (Table 4). Such result is not surprising as iron is limiting diatom growth over about 40% of the global ocean in HAMOCC5 whereas silicate limitation is dominating only in the North Atlantic and in some small regions of the Southern Ocean representing about 5% of the world ocean. This sensitivity highlights the needs for a better understanding of the processes controlling the iron biogeochemistry. This is especially critical for the $\frac{Fe}{C}$ for phytoplankton and the solubility of deposited iron, both leading to the largest changes in model results. Nevertheless, our model may underestimate the role of silica as the simulated extent of Si-limited areas is probably underestimated in the Southern Ocean (see section 4.1).

[58] Results from the several sensitivity experiments we performed exhibit an interesting behavior: A relief from iron or silicon stress induces an overall decrease in total primary production. At first, one would have expected exactly the opposite. A weaker iron or silicon limitation benefits mainly to diatoms whose global abundance increases. But this fertilizing effect on diatoms is more than balanced by a decrease in nanophytoplankton primary production. In fact, the larger diatom-based biological activity results in a more efficient export of organic matter into the deep ocean (see Figure 11b). Thus surface waters are more exhausted in phosphate and the extent of oligotrophic areas is increasing. Such an inverse relationship between iron stress and the sea surface phosphate inventory was shown by *Archer and Johnson* [2000] in their sensitivity experiments on atmospheric deposition of
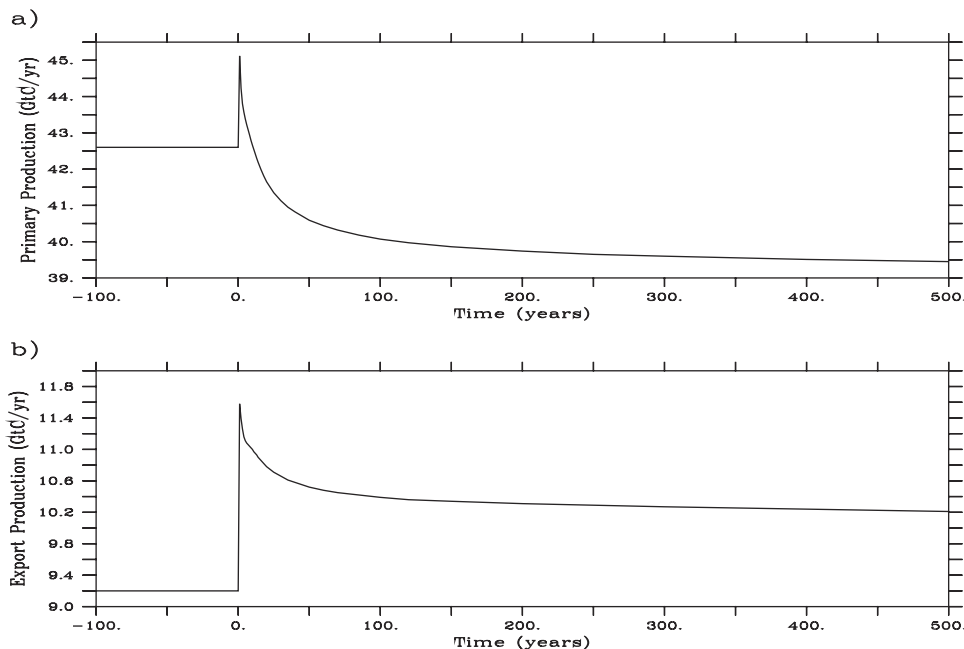
Figure 11. Time evolution of the globally integrated annual (a) primary production and (b) export production after switching the solubility of deposited iron from 1% to 10%.

iron and on the bioavailability of deposited iron (their Figures 8 and 9). The increased oligotrophy of surface waters of the world ocean explains the weaker nanophytoplankton primary production.

[59] In Figure 11, we have displayed the time evolution of the global primary and export productions after switching the solubility of deposited iron from the standard 1% to 10%. The first year, the total primary production jumps to its maximum value of 45.1 GtC yr^{-1}, that is 6% more than in the standard run. Afterwards, primary production decreases as phosphate becomes more exhausted from surface waters due to a more intense export production. By year 12, primary production falls below the 42.6 GtC yr^{-1} simulated in the standard model. Export production exhibits a similar behavior with a strong increase the first year followed by a slow decline. Nevertheless, the steady-state value to which export production tends is significantly higher than in the standard simulation. With their model, *Moore et al.* [2002a] have conducted similar experiments on iron solubility. Performing 3-year-long sensitivity runs, they have concluded that increased iron supply should result both in an enhanced primary and export production. Our tests suggest that these runs are much too short and give only an answer on the short-term response of the ocean that may be very different from the longer-term trend.

5. Conclusions

[60] We have presented results from a coupled biological-physical model of the world ocean. The biological model, HAMOCC5, includes two compartments for phytoplankton and two compartments for zooplankton. In addition to phosphate, potential limitation of phytoplankton growth by silicate and iron has been considered as these nutrients

may play a critical role in HNLC regions. A single set of parameters is used over the global domain. The model is generally able to reproduce the general patterns of surface chlorophyll and major nutrients. In particular, low surface chlorophyll concentrations are predicted over two of the three major HNLC regions, i.e. the equatorial Pacific and the Southern Ocean. This is an improvement in comparison with previous modeling studies using simpler biological schemes [*Six and Maier-Reimer*, 1996; *Aumont et al.*, 2002; *Palmer and Totterdell*, 2001]. However, in the North Pacific, HAMOCC5 largely underestimates the average levels of phosphate and silicate, mainly because of a faulty representation of the ocean dynamics.

[61] The model explains the low chlorophyll concentrations observed in HNLC regions by the lack of iron which prevents diatoms from growing. Nanophytoplankton is kept in control by an efficient grazing by microzooplankton. Thus, this result supports the traditional hypothesis that in HNLC areas, in particular in the equatorial Pacific, phytoplankton is both limited by iron and grazing. Areas limited by silicate availability encompass only 5% of the world ocean in HAMOCC5. However, this extent is certainly underestimated as observations have shown wide silicon limitation North of the Polar Front in the Southern Ocean, a pattern largely missing in our model results.

[62] The predicted global iron budget can be characterized as follows. Phytoplankton consumes about 18×10^9 mol Fe yr^{-1} corresponding to a mean $\frac{Fe}{C}$ of 5.1×10^{-6} mol.mol^{-1} very close to the 5×10^{-6} mol.mol^{-1} estimated by *Johnson et al.* [1997] from observations. We neglected potential iron input from coastal zones because of the too coarse resolution of the dynamic model and because of the uncertainties in the coastal input and processes. The total upward supply of iron by ocean circulation is evaluated to

4.5×10^9 mol Fe yr^{-1} whereas atmospheric deposition brings 1.4×10^9 mol Fe yr^{-1} to phytoplankton assuming a 1% solubility for dust-iron. About 1×10^9 mol Fe yr^{-1} is transported back to the sub-surface without having being assimilated by phytoplankton. Thus, the ocean carries with it about 75% of the phytoplankton demand for new iron. This finding is in agreement with the studies by *Archer and Johnson* [2000] and *Moore et al.* [2002a] and much higher than the 7–40% estimated by *Fung et al.* [2000].

[63] This study is of course spoilt by many uncertainties. A sensitivity analysis conducted onto the parameterizations we assumed for the silicon and iron cycles has shown that the model results are mostly sensitive to our lack of knowledge for the biogeochemistry of iron. Furthermore, it has revealed a rather interesting inverse relationship between the intensity of the iron stress and the global total primary production. An increased iron supply induces a decline in primary production because the higher export production resulting from a larger diatoms abundance produces a larger spatial extent of oligotrophic areas. *Fung et al.* [2000] have listed in their conclusion a number of priorities that should help to better understand the iron cycle in the upper ocean. We strongly support them.

References

André, J. M., Télédétection spatiale de la couleur de la mer: Algorithme d'inversion des mesures du Coastal Zone Color Scanner, Applications à l'étude de la Méditerrannée occidentale, Ph.D. thesis, Université Marie et Pierre Curie, Paris, France, 1990.

Antoine, D., J. M. André, and A. Morel, Oceanic primary production, 2, Estimation at global scale from satellite (coastal zone color scanner) chlorophyll, *Global Biogeochem. Cycles*, 10, 57–69, 1996.

Archer, D. E., and K. S. Johnson, A model of iron cycle in the ocean, *Global Biogeochem. Cycles*, 14, 269–279, 2000.

Aumont, O., J. C. Orr, P. Monfray, G. Madec, and E. Maier-Reimer, Nutrient trapping in the equatorial pacific: The ocean circulation solution, *Global Biogeochem. Cycles*, 13, 351–371, 1999.

Aumont, O., S. Belviso, and P. Monfray, Dimethylsulfoniopropionate (dmsp) and dimethylsulfide (dms) sea surface distributions simulated from a global three-dimensional ocean carbon cycle model, *J. Geophys. Res.*, 107, 3029, doi:10.1029/1999JC000111, 2002.

Behrenfeld, M. J., and P. G. Falkowski, A consumer's guide to phytoplankton primary productivity models, *Limnol. Oceanogr.*, 42, 1479–1491, 1997.

Belviso, S., H. Claustre, and J. C. Marty, Evaluation of the utility of chemico-taxonomic pigments as a surrogate for particulate DMSP, *Limnol. Oceanogr.*, 46, 989–995, 2001.

Blain, S., A. Leynaert, P. Tréguer, M. J. Chrétiennot-Dinet, and M. Rodier, Biomass, growth rates and limitation of Equatorial Pacific diatoms, *Deep Sea Res., Part I*, 44, 1255–1275, 1997.

Blain, S., et al., A biogeochemical study of the island mass effect in the context of the iron hypothesis: Kerguelen Islands, Southern Ocean, *Deep Sea Res., Part I*, 48, 163–187, 2001.

Bodungen, B. V., and P. Kähler, Dissolved organic carbon in the Atlantic Ocean: Regional and seasonal patterns, *EOS Trans. AGU*, 75(3), Ocean Sci. Meet. Suppl., 106, 1994.

Boyd, P., and P. Harrison, Phytoplankton dynamics in the NE subarctic Pacific, *Deep Sea Res., Part II*, 46, 2405–2432, 1999.

Boyd, P., J. LaRoche, M. Gall, R. Frew, and R. M. L. McKay, Role of iron, light, and silicate in controlling algal biomass in subantarctic waters SE of New Zealand, *J. Geophys. Res.*, 104, 13,395–13,408, 1999.

Boyd, P. W., et al., A mesoscale phytoplankton bloom in the polar Southern Ocean stimulated by iron fertilization, *Nature*, 407, 695–702, 2000.

Bracher, A. U., B. M. A. Kroon, and M. I. Lucas, Primary production, physiological state and composition of phytoplankton in the Atlantic Sector of the Southern Ocean, *Mar. Ecol. Prog. Ser.*, 190, 1–16, 1999.

Bruland, K. W., K. J. Orians, and J. P. Cowen, Reactive trace metals in the stratified North Pacific, *Geochim. Cosmochim. Acta*, 58, 3171–3182, 1994.

Brzezinski, M. A., Cell-cycle effects on the kinetics of silicic acid uptake and resource competition among diatoms, *J. Plankton Res.*, 14, 1511–1539, 1992.

Buck, K. R., and F. P. Chavez, Diatom aggregates from the open ocean, *J. Plankton Res.*, 16, 1449–1457, 1994.

Carlson, C. A., H. W. Ducklow, and A. F. Michaels, Annual flux of dissolved organic carbon from the euphotic zone in the northwestern Sargasso Sea, *Nature*, 371, 405–408, 1994.

Chavez, F. P., K. R. Buck, K. H. Coale, J. H. Martin, G. R. DiTullio, N. A. Welschmeyer, A. C. Jacobson, and R. T. Barber, Growth rates, grazing, sinking and iron limitation of equatorial Pacific phytoplankton, *Limnol. Oceanogr.*, 36, 1816–1863, 1991.

Christian, J. R., M. A. Verschell, R. Murtugudde, A. J. Busalacchi, and C. R. McClain, Biogeochemical modelling of the tropical Pacific Ocean, I, Seasonal and interannual variability, *Deep Sea Res., Part II*, 49, 509–543, 2002.

Coale, K. H., et al., A massive phytoplankton bloom induced by an ecosystem-scale iron fertilization experiment in the equatorial Pacific Ocean, *Nature*, 383, 495–501, 1996.

Conkright, M. E., S. Levitus, and T. P. Boyer, *NOAA Atlas NESDIS 1: World Ocean Atlas 1994*, vol. 1, *Nutrients*, Natl. Oceanic and Atmos. Admin., Silver Spring., Md., 1994.

Dafner, E. V., and N. V. Mordasova, Influence of biotic factors on the hydrochemical structure of surface water in the Polar Frontal Zone of the Atlantic Antarctic, *Mar. Chem.*, 45, 137–148, 1994.

Dagg, M., Grazing by the copepod community does not control phytoplankton production in the Subarctic Pacific Ocean, *Prog. Oceanogr.*, 32, 163–183, 1993.

Dale, T., F. Rey, and B. R. Heimdal, Seasonal development of phytoplankton at a high latitude oceanic site, *Sarsia*, 84, 419–435, 1999.

Dam, H. G., C. A. Miller, and S. H. Jonasdottir, The trophic role of mesozooplankton at 47°N, 20°W during the North Atlantic Bloom Experiment, *Deep Sea Res.*, 40, 197–212, 1993.

de Baar, H. J. W., A. G. J. Buma, R. F. Nolting, G. C. Cadée, G. Jacques, and P. Tréguer, On iron limitation of the Southern Ocean: Experimental observations in the Weddell and Scotia Seas, *Mar. Ecol. Prog. Ser.*, 65, 105–122, 1990.

de Baar, H. J. W., J. T. M. de Jong, D. C. E. Bakker, B. M. Löscher, C. Veth, U. Bathmann, and V. Smetacek, Importance of iron for phytoplankton spring blooms and CO_2 drawdown in the Southern Ocean, *Nature*, 373, 412–415, 1995.

de Baar, H. J. W., J. T. M. de Jong, R. F. Nolting, K. R. Timmermans, M. A. van Leeuwe, U. Bathmann, M. Rutgers van der Loeff, and J. Sildam, Low dissolved Fe and the absence of diatom blooms in remote Pacific waters of the Southern Ocean, *Mar. Chem.*, 66, 1–34, 1999.

Doney, S. C., D. M. Glover, and R. G. Najjar, A new coupled one-dimensional biological-physical model for the upper ocean: Applications to the JGOFS Bermuda Atlantic Time-series Study (BATS) site, *Deep Sea Res., Part II*, 43, 591–624, 1996.

Duce, R. A., and N. W. Tindale, Atmospheric transport of iron and its deposition in the ocean, *Limnol. Oceanogr.*, 36, 1715–1726, 1991.

Ducklow, H. W., D. L. Kirchman, H. L. Quinby, C. A. Carlson, and H. G. Dam, Stocks and dynamics of bacterioplankton carbon during the spring bloom in the eastern North Atlantic Ocean, *Deep Sea Res.*, 40, 245–263, 1993.

Dugdale, R. C., and F. P. Wilkerson, Silicate regulation of new production in the equatorial Pacific upwelling, *Nature*, 391, 270–273, 1998.

Eppley, R. W., Temperature and phytoplankton growth in the sea, *Fish. Bull.*, 70, 1063–1085, 1972.

Eppley, R. W., and B. J. Peterson, Particulate organic matter flux and planktonic new production in the deep ocean, *Nature*, 282, 677–680, 1979.

Fasham, M. J. R., H. W. Ducklow, and S. M. McKelvie, A nitrogen-based model of plankton dynamics in the oceanic mixed layer, *J. Mar. Res.*, 48, 591–639, 1990.

Fiala, M., E. Kopczynska, C. Jeandel, L. Oriol, and G. Vetion, Seasonal and interannual variability of size-fractionated phytoplankton biomass and community structure at station Kerfix, off the Kerguelen Islands, Antarctica, *J. Plankton Res.*, 20, 1341–1356, 1998.

Fitzwater, S. E., K. H. Coale, R. M. Gordon, K. S. Johnson, and M. E. Ondrusek, Iron deficiency and phytoplankton growth in the equatorial Pacific, *Deep Sea Res., Part II*, 43, 995–1015, 1996.

Franck, V. M., M. A. Brzezinski, K. H. Coale, and D. M. Nelson, Iron and silicic acid concentrations regulate Si uptake north and south of the Polar Frontal Zone in the Pacific Sector of the Southern Ocean, *Deep Sea Res., Part II*, 47, 3315–3338, 2000.

Froneman, P. W., E. A. Pakhomov, R. Perissinotto, and C. D. McQuaid, Zooplankton structure and grazing in the Atlantic sector of the Southern Ocean in late austral summer 1993, 2, Biochemical zonation, *Deep Sea Res., Part I*, 47, 1687–1702, 2000.

Frost, B. W., The role of grazing in nutrient-rich areas of the open sea, *Limnol. Oceanogr.*, 36, 1616–1630, 1991.

Fung, I. Y., S. K. Meyn, I. Tegen, S. C. Doney, J. G. John, and K. B. Bishop, Iron supply and demand in the upper ocean, *Global Biogeochem. Cycles*, 14, 281–295, 2000.

Gaspar, P., Y. Gregoris, and J. M. Lefevre, A simple eddy kinetic energy model for simulations of the ocean vertical mixing: Tests at station Papa and Long-Term Upper Ocean Study Site site, *J. Geophys. Res.*, 95, 16,179–16,193, 1990.

Gerringa, L. J. A., H. J. W. de Baar, and K. R. Timmermans, A comparison of iron limitation of phytoplankton in natural oceanic waters and laboratory media conditioned with EDTA, *Mar. Chem.*, 68, 335–346, 2000.

Gifford, D. J., P. R. Garrahan, and E. Martin, Grazing by microzooplankton and mesozooplankton in the high-latitude North Atlantic Ocean: Spring versus summer dynamics, *J. Geophys. Res.*, 100, 6665–6675, 1995.

Gordon, R. M., K. H. Coale, and K. S. Johnson, Iron distributions in the equatorial Pacific: Implications for new production, *Limnol. Oceanogr.*, 42, 419–431, 1997.

Jacques, G., Some ecophysiological aspects of the antarctic phytoplankton, *Polar Biol.*, 2, 27–33, 1983.

Jassby, A. D., and T. Platt, Mathematical formulation of the relationship between photosynthesis and light for phytoplankton, *Limnol. Oceanogr.*, 21, 540–547, 1976.

Jickells, T. D., and L. J. Spokes, Atmospheric iron inputs to the oceans, in *Biogeochemistry of Fe in Seawater*, edited by D. R. Turner and K. A. Hunter, pp. 85–121, Wiley Intersci., New York, 2001.

Johnson, K. S., R. M. Gordon, and K. H. Coale, What controls dissolved iron concentrations in the world ocean?, *Mar. Chem.*, 57, 137–161, 1997.

Joint, I., A. Pomroy, G. Savidge, and P. Boyd, Size-fractionated primary productivity in the northeast Atlantic in May–June 1989, *Deep Sea Res., Part II*, 40, 423–440, 1993.

Kamykowski, D., and S. J. Zentara, Circumpolar plant nutrient covariation in the Southern Ocean: Patterns and processes, *Mar. Ecol. Prog. Ser.*, 58, 101–111, 1989.

Killworth, P. D., Deep convection in the World Ocean, *Rev. Geophys.*, 21, 1–26, 1983.

Lancelot, C., E. Hannon, S. Becquevort, C. Veth, and H. J. W. de Baar, Modelling phytoplankton blooms and related carbon export production in the Southern Ocean: Application to the Atlantic sector in Austral spring 1992, *Deep Sea Res., Part I*, 47, 1621–1662, 2000.

Landry, M. R., J. D. Kirshtein, and J. R. Constantinou, A refined dilution technique for measuring the community grazing impact of microzooplankton, with experimental tests in the central equatorial Pacific, *Mar. Ecol. Prog. Ser.*, 120, 53–63, 1995.

Landry, M. R., M. E. Ondrusek, S. J. Tanner, S. L. Brown, J. Constantinou, R. R. Bidigare, K. H. Coale, and S. Fitzwater, Biological response to iron fertilization in the eastern equatorial Pacific (IronEx II), I, Microplankton community abundances and biomass, *Mar. Ecol. Prog. Ser.*, 201, 27–42, 2000.

Leonard, C. L., C. R. McClain, R. Murtugudde, E. E. Hoffmann, and L. W. Harding, An iron-based ecosystem model of the central equatorial Pacific, *J. Geophys. Res.*, 104, 1325–1341, 1999.

Lévy, M., L. Mémery, and G. Madec, The onset of a bloom after deep winter convection in the northwestern Mediterranean sea: Mesoscale process study with a primitive equation model, *J. Mar. Syst.*, 16, 7–21, 1998.

Lochte, K., H. W. Ducklow, M. J. R. Fasham, and C. Stienen, Plankton succession and carbon cycling at 47°N 20°W during the JGOFS North Atlantic Bloom Experiment, *Deep Sea Res.*, 40, 91–114, 1993.

Longhurst, A., S. Sathyendranath, T. Platt, and C. Caverhill, An estimate of global primary production in the ocean from satellite radiometer data, *J. Plankton Res.*, 17, 1245–1271, 1995.

Maier-Reimer, E., Geochemical cycles in an ocean general circulation model: Preindustrial tracer distributions, *Global Biogeochem. Cycles*, 7, 645–677, 1993.

Maier-Reimer, E., U. Mikolajewicz, and K. Hasselmann, Mean circulation of the Hamburg LSG OGCM and its sensitivity to the thermohaline surface forcing, *J. Phys. Oceanogr.*, 23, 731–757, 1993.

Malone, T. C., Algal size, in *The Physiological Ecology of Phytoplankton*, edited by I. Morris, pp. 433–463, Blackwell, Malden, Mass., 1980.

Marañón, E., P. M. Holligan, M. Varuela, B. Mouriño, and A. J. Bale, Basin-scale variability of phytoplankton biomass, production and growth in the Atlantic Ocean, *Deep Sea Res., Part I*, 47, 825–857, 2000.

Martin, J. H., and S. E. Fitzwater, Iron deficiency limits phytoplankton growth in the northeast Pacific subarctic, *Nature*, 331, 341–343, 1988.

Martin, J. H., S. E. Fitzwater, R. M. Gordon, C. N. Hunter, and S. J. Tanner, Iron, primary production and carbon-nitrogen flux studies during the JGOFS North Atlantic Bloom Experiment, *Deep Sea Res., Part II*, 40, 115–134, 1993.

McGillicuddy, O. J., A. R. Robinson, D. A. Siegel, H. W. Jannasch, R. Johnson, T. D. Dickey, H. McNell, A. F. Michaels, and A. H. Knap, Influence of mesoscale eddies on new production in the Sargasso Sea, *Nature*, 394, 263–266, 1998.

Mitchell, B. G., E. A Brody, O. Holm-Hansen, C. McClain, and J. K. B. Bishop, Light limitation of phytoplankton biomass and macronutrient utilisation in the Southern Ocean, *Limnol. Oceanogr.*, 36, 1662–1677, 1991.

Moore, J. K., S. C. Doney, D. M. Glover, and I. Y. Fung, Iron cycling and nutrient limitation patterns in surface waters of the world ocean, *Deep Sea Res., Part II*, 49, 463–507, 2002a.

Moore, J. K., S. C. Doney, J. A. Kleypas, D. M. Glover, and I. Y. Fung, An intermediate complexity marine ecosystem model for the global domain, *Deep Sea Res., Part II*, 49, 403–462, 2002b.

Morales, C. E., A. Bedo, R. P. Harris, and P. R. G. Tranter, Grazing of copepod assemblages in the north-east Atlantic: The importance of the small size fraction, *J. Plankton Res.*, 13, 455–472, 1991.

Muggli, D. L., M. Lecourt, and P. J. Harrison, Effects of iron and nitrogen source on the sinking rate, physiology and metal composition of an oceanic diatom from the subarctic Pacific, *Mar. Ecol. Prog. Ser.*, 132, 215–227, 1996.

Murray, J. W., R. T. Barber, M. R. Roman, M. P. Bacon, and R. A. Feely, Physical and biological controls on carbon cycling in the equatorial Pacific, *Science*, 266, 58–65, 1994.

Nelson, D. M., and W. O. Smith, Sverdrup revisited: Critical depths, maximum chlorophyll levels, and the control of the Southern Ocean productivity by the irradiance mixing regime, *Limnol. Oceanogr.*, 36, 1650–1661, 1991.

Nelson, D. M., and P. Tréguer, Role of silicon as a limiting nutrient to Antarctic diatoms: Evidence from kinetic studies in the Ross Sea ice-edge zone, *Mar. Ecol. Prog. Ser.*, 80, 255–264, 1992.

Nelson, D. M., P. Tréguer, M. A. Brzezinski, A. Leynaert, and B. Quéguiner, Production and dissolution of biogenic silica in the ocean: Revised global estimates, comparison with regional data and relationship to biogenic sedimentation, *Global Biogeochem. Cycles*, 9, 359–372, 1995.

Nolting, R. F., L. Gerringa, R. Swagerman, K. R. Timmermans, and H. J. W. de Baar, Fe(III) speciation in the high nutrient low chlorophyll Pacific region of the Southern Ocean, *Mar. Chem.*, 62, 335–352, 1998.

Oschlies, A., and V. Garçon, Eddy-induced enhancement of primary production in a model of the North Atlantic Ocean, *Nature*, 394, 266–269, 1998.

Palmer, J. R., and I. J. Totterdell, Production and export in a global ocean ecosystem model, *Deep Sea Res., Part I*, 48, 1169–1198, 2001.

Pondaven, P., C. Fravalo, D. Ruiz-Pino, P. Tréguer, B. Quéguiner, and C. Jeandel, Modelling the silica pump in the Permanently Open Ocean Zone of the Southern Ocean, *J. Mar. Syst.*, 17, 587–619, 1998.

Pondaven, P., D. Ruiz-Pino, J. N. Druon, C. Fravalo, and P. Tréguer, Factors controlling silicon and nitrogen biogeochemical cycles in high nutrient, low chlorophyll systems (the Southern Ocean and the North Pacific): Comparison with a mesotrophic system (the North Atlantic), *Deep Sea Res., Part I*, 46, 1923–1968, 1999.

Rue, E. L., and K. W. Bruland, Complexation of iron(III) by natural organic ligands in the Central North Pacific as determined by a new competitive ligand equilibration/absorptive cathodic stripping voltametric approach, *Mar. Chem.*, 50, 117–138, 1995.

Sakshaug, E., and O. Holm-Hansen, Chemical composition of *Skeletonema Costatum* and *Pavlova* (*Monochrysis lutheri*) as a function of nitrate-, phosphate- and iron-limited growth, *J. Exp. Mar. Biol. Ecol.*, 29, 1–34, 1977.

Savidge, G., P. Boyd, A. Pomroy, D. Harbour, and I. Joint, Phytoplankton production and biomass estimates in the northeast Atlantic Ocean, May–June 1990, *Deep Sea Res., Part I*, 42, 599–617, 1995.

Scharek, R., M. Latasa, D. M. Karl, and R. R. Bidigare, Temporal variations in diatom abundance and downward vertical flux in the oligotrophic North Pacific gyre, *Deep Sea Res., Part I*, 46, 1051–1075, 1999.

Semeneh, M., F. Dehairs, M. Elskens, M. E. M. Baumann, E. E. Kopczynska, C. Lancelot, and L. Goeyens, Nitrogen uptake regime and phytoplankton community structure in the Atlantic and Indian sectors of the Southern Ocean, *J. Mar. Syst.*, 17, 159–177, 1998.

Sieracki, M. E., P. G. Verity, and D. K. Stroecker, Plankton community response to sequential silicate and nitrate depletion during the 1989 North Atlantic spring bloom, *Deep Sea Res., Part II*, *40*, 213–225, 1993.

Six, K. D., and E. Maier-Reimer, Effects of plankton dynamics on seasonal carbon fluxes in an ocean general circulation model, *Global Biogeochem. Cycles*, *10*, 559–583, 1996.

Smetacek, V., Role of sinking in diatom life-history cycles: Ecological, evolutionary and geological significance, *Mar. Biol.*, *84*, 239–251, 1985.

Sohrin, Y., S. Iwamoto, M. Matsui, H. Obata, E. Nakayama, K. Suzuki, and M. Ishii, The distribution of Fe in the Australian sector of the Southern Ocean, *Deep Sea Res., Part I*, *47*, 55–84, 2000.

Sommer, U., Nitrate and silicate competition among Antarctic phytoplankton, *Mar. Biol.*, *91*, 345–351, 1986.

Suess, E., Particulate organic carbon flux in the ocean-surface productivity and oxygen utilization, *Nature*, *288*, 260–263, 1980.

Sullivan, C. W., K. R. Arrigo, C. R. McClain, J. C. Comiso, and J. Firestone, Distributions of phytoplankton blooms in the Southern Ocean, *Science*, *262*, 1832–1837, 1993.

Sunda, W. G., and S. A. Huntsman, Interrelated influence of iron, light and cell size on marine phytoplankton growth, *Nature*, *390*, 389–392, 1997.

Tegen, I., and I. Fung, Contribution to the atmospheric mineral aerosol load from land surface modification, *J. Geophys. Res.*, *100*, 18,707–18,726, 1995.

Toggweiler, J. R., and B. Samuels, New radiocarbon constraints on the upwelling of abyssal water to the ocean's surface, in *The Global Carbon Cycle*, *NATO ASI Ser., Ser. I*, vol. 15, edited by M. Heimann, pp. 333–366, Springer-Verlag, New York, 1993.

Tréguer, P., and A. J. van Bennekom, The annual production of biogenic silica in the Antarctic Ocean, *Mar. Chem.*, *35*, 477–488, 1991.

Tréguer, P., D. M. Nelson, A. J. Van Bennekom, D. J. DeMaster, A. Leynaert, and B. Quéguiner, The silica balance in the World Ocean: A reestimate, *Science*, *268*, 375–379, 1995.

van den Berg, C. M. G., A. G. A. Mercks, and E. K. Duursma, Organic complexation and its control of the dissolved concentrations of copper and zinc in the Scheldt Estuary, *Estuarine Coast. Shelf Sci.*, *24*, 785–797, 1995.

Verity, P. G., D. K. Stoecker, M. E. Siriacki, and J. R. Nelson, Microzooplankton grazing of primary production at 140oW in the equatorial Pacific, *Deep Sea Res., Part II*, *43*, 1227–1255, 1996.

Wheehler, P. A., New production in the Subarctic Pacific Ocean: Net changes in nitrate concentrations, rates of nitrate assimilation and accumulation of particulate organic nitrogen, *Prog. Oceanogr.*, *32*, 137–161, 1993.

Wright, S. W., and R. L. van den Enden, Phytoplankton community structure and stocks in the East Antarctic marginal ice zone (BROKE survey, January–March 1996) determined by CHEMTAX analysis of HPLC pigment signatures, *Deep Sea Res., Part II*, *47*, 2363–2400, 2000.

Wu, J., and G. W. Luther, Complexation of Fe(III) by natural organic ligands in the Northwest Atlantic Ocean by a competitive ligand equilibration method and a kinetic approach, *Mar. Chem.*, *50*, 159–177, 1995.

————————————

O. Aumont, Laboratoire d'Océanographie Dynamique et de Climatologie, Unité mixte CNRS/IRD/UPMC, 4 place Jussieu, F-75252 Paris, France. (aumont@lodyc.jussieu.fr)

S. Blain, Institut Universitaire Européen de la Mer, Technopole Brest-Iroise, Place Copernic, F-29280 Plouzané, France. (blain@univ-brest.fr)

E. Maier-Reimer, Max-Planck Institut fuer Meteorologie, Bundesstrasse 55, D-20146 Hamburg, Germany. (maier-reimer@dkrz.de)
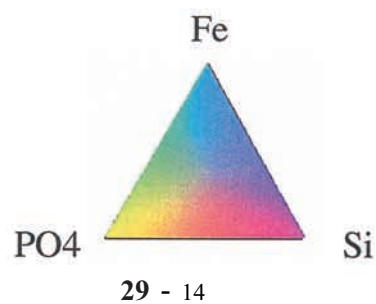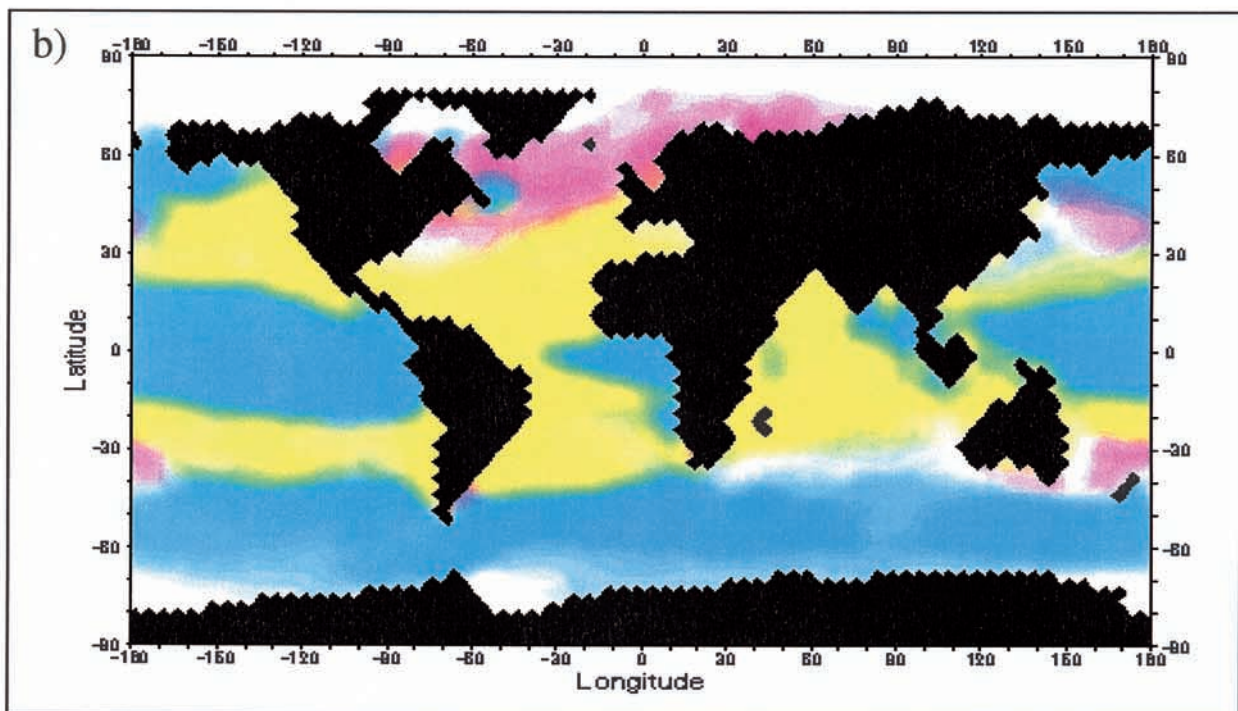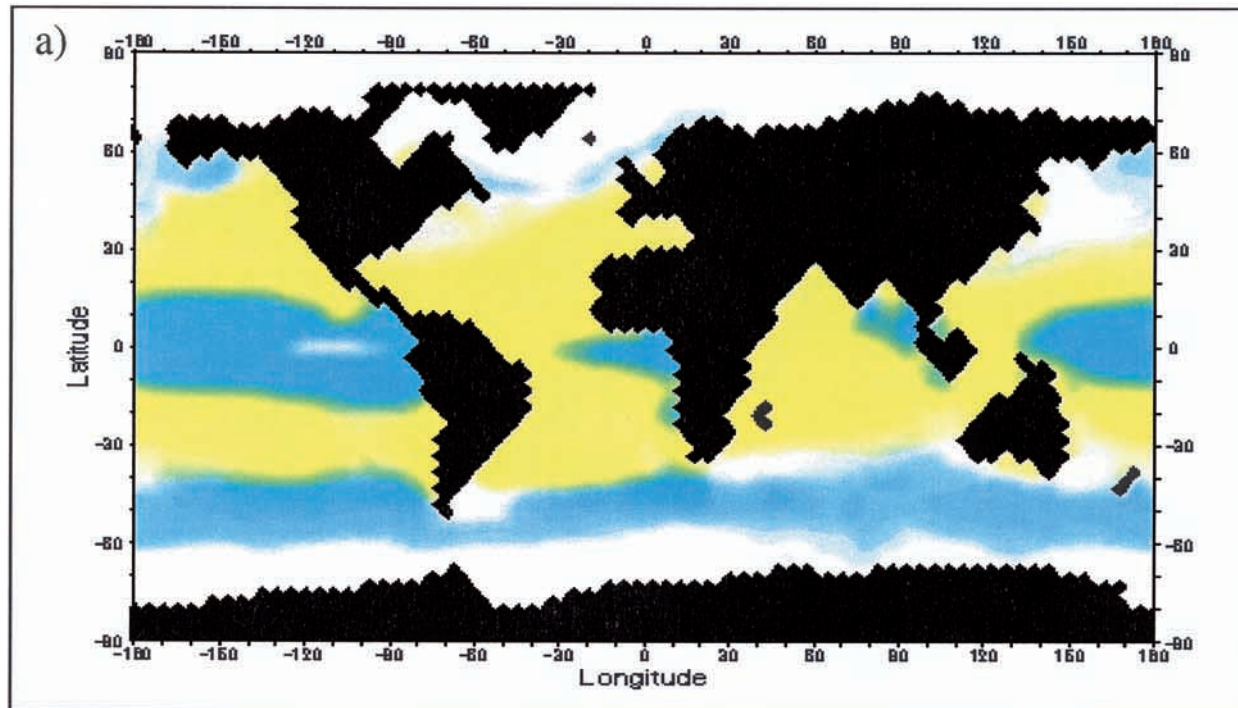
P. Monfray, Laboratoire des Sciences du Climat et de l'Environnement, CE Saclay, L'Orme des Merisiers, F-91191 Gif-sur-Yvette, France. (monfray@lsce.saclay.cea.fr)
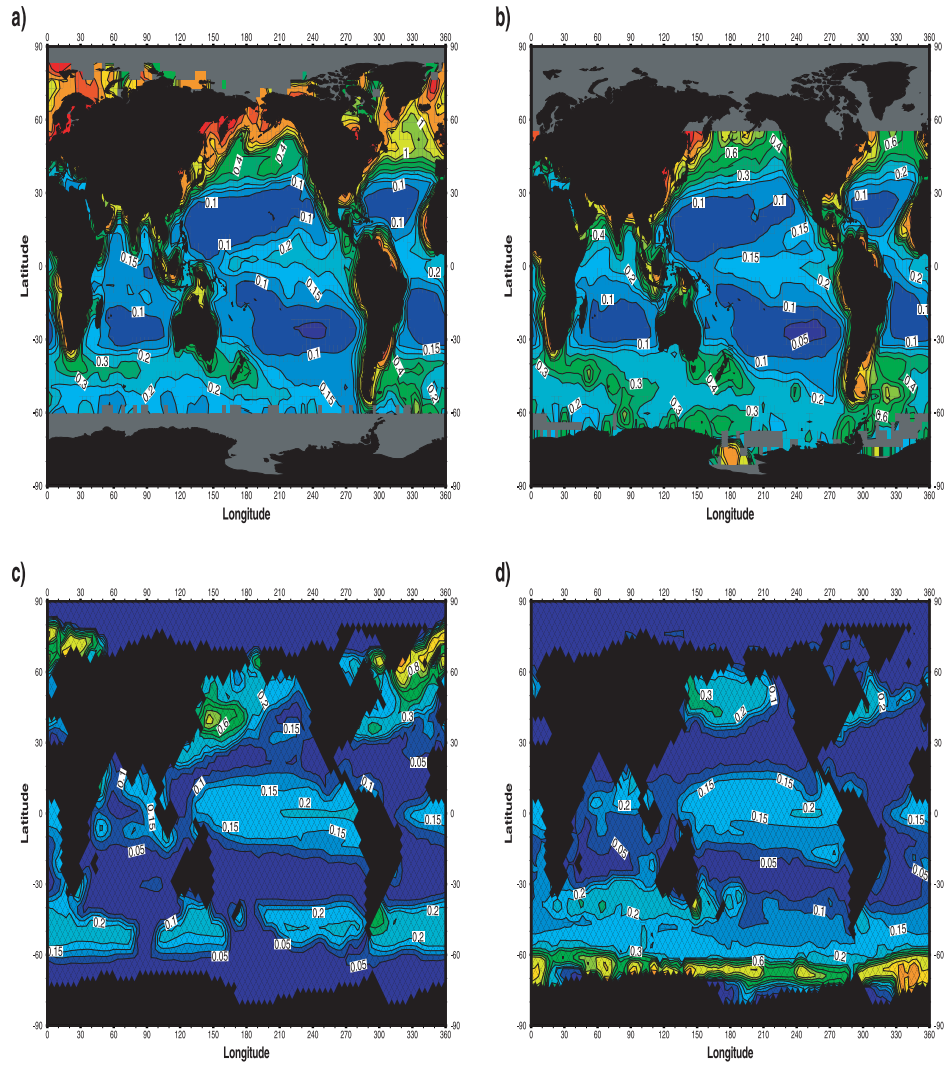
Figure 3. Monthly mean of the chlorophyll distribution (in mg Chl m^{-3}) from SeaWIFS and HAMOCC5 in May (a and c, respectively) and November (b and d, respectively). Satellite derived data have been interpolated onto a regular grid with a 3.5° horizontal resolution corresponding to the LSG model resolution. Isolines are at 0.05, 0.1, 0.15, 0.2, 0.3, 0.4, 0.6, 0.8, 1, 2, 4, and 6.

Figure 8. (opposite) Nutrient colimitations of (a) nanophytoplankton and (b) diatoms by the three modeled nutrients. The colors denote the temporal occurrence of the limitation by the different nutrients. Thus a full yellow color means that the ecosystem is limited by phosphate all year long. A mix of two different colors means that over the year, the ecosystem is limited by two different nutrients. The limiting nutrient is computed from $L_{P,D}$ (see Table 2). The intensity of the colors is modulated to give extra-information both on the magnitude of the nutrient limitations and on the light limitation. Paler colors mean that during part of the year, biological production is either not limited by nutrients or is light limited. Phytoplankton growth is considered to be light limited when the convective depth is deeper than 100 m. Furthermore, the three modeled nutrients are considered not to be limiting when the Michaelis-Menten function is larger than 2/3. These maps have been computed from monthly mean fields.